HHS Public Access

Author manuscript

J Immunol. Author manuscript; available in PMC 2025 January 15.

Published in final edited form as:

J Immunol. 2024 January 15; 212(2): 302–316. doi:10.4049/jimmunol.2300319.

IL-17A orchestrates ROS-HIF1α-mediated metabolic reprogramming in psoriasis

Bhavuk Dhamija[*,1], **Soumitra Marathe**[*,1], **Vinanti Sawant**[*], **Moumita Basu**[*], **Diksha Attrish**[*], **Ditipriya Mukherjee**[*], **Sushant Kumar**[*], **Medha Gayathri J Pai**[*], **Siddhi Wad**[*], **Abhijeet Sawant**[†], **Chitra Nayak**[‡], **KV Venkatesh**[§], **Sanjeeva Srivastava**[*], **Steven R. Barthel**[¶,2,3], **Rahul Purwar**[*,2,3]

[*]Department of Biosciences and Bioengineering, IIT Bombay, Mumbai, India.

[†]Plastic Surgery Department, TNMC and BYL Nair Charitable Hospital, Mumbai, India.

[‡]Skin and Venereal Diseases Department, TNMC and BYL Nair Charitable Hospital, Mumbai, India.

[§]Department of Chemical Engineering, IIT Bombay, Mumbai, India.

[¶]Department of Dermatology, Brigham and Women's Hospital, Harvard Medical School, Boston, MA, USA.

Abstract

Immune cell-derived IL-17A is one of the key pathogenic cytokines in psoriasis, an immuno-metabolic disorder. While IL-17A is an established regulator of cutaneous immune cell biology, its functional and metabolic effects on non-immune cells of the skin, particularly keratinocytes, have not been comprehensively explored. Using multi-omics profiling and systems biology-based approaches, we systematically uncover new roles for IL-17A in the metabolic reprogramming of human primary keratinocytes (HPKs). High-throughput LC-MS/MS and NMR spectroscopy revealed IL-17A-dependent regulation of multiple HPK proteins and metabolites of carbohydrate and lipid metabolism. Systems-level Mitocore modeling using flux-balance analysis identified IL-17A-mediated increases in HPK glycolysis, glutaminolysis, and, lipid uptake, which were validated using biochemical cell-based assays and stable isotope resolved metabolomics (SIRM). IL-17A treatment triggered downstream mitochondrial reactive oxygen (mROS) and HIF1α

[3]Correspondence to Drs. Steven R. Barthel or Rahul Purwar, sbarthel@bwh.harvard.edu or purwarrahul@iitb.ac.in.

[1]B.D. and S.M. contributed equally to this study.

[2]S.R.B. and R.P. contributed equally to this study

AUTHOR CONTRIBUTIONS

Conceptualization: R.P., B.D., and S.M.; Data curation: B.D., S.M.; Formal Analysis: B.D., S.M., M.B., M.G.P.; Funding acquisition: R.P., K.V.V., S.R.B.; Investigation: B.D., S.M., M.B., M.G.P., S.K., V.S., D.M., D.A., S.W.; Methodology: B.D., S.M., M.B.; Project administration: R.P.; Resources: B.D., S.M., S.K., V.S., S.W., D.M., D.A., R.P., A.S., and C.N.; Supervision: K.V.V., S.R.B, S. Sri., and R.P.; Validation: B.D., S.M., M.B.; Visualization: B.D., S.M., M.B.; Writing original draft: R.P., S.R.B., B.D., S.M., and M.B.; Review & editing: R.P., S.R.B., B.D., S.M., and M.B.

ETHICS STATEMENT

Healthy skin specimens were collected at the Plastic Surgery Department of B.Y.L. Nair Charitable Hospital, Mumbai with the approval of the Institute Ethics Committee (IEC) of IIT Bombay and B.Y.L. Nair Charitable Hospital, Mumbai (Approval ID: SVD/47).

CONFLICT OF INTEREST

The authors have declared that they have no conflict of interest.

expression and resultant HPK proliferation, consistent with the observed elevation of these downstream effectors in the epidermis of patients with psoriasis. Pharmacological inhibition of HIF1α or ROS reversed IL-17A-mediated glycolysis, glutaminolysis, lipid uptake, and HPK hyperproliferation. These results identify keratinocytes as important target cells of IL-17A and reveal its involvement in multiple downstream metabolic reprogramming pathways in human skin.

Graphical Abstract

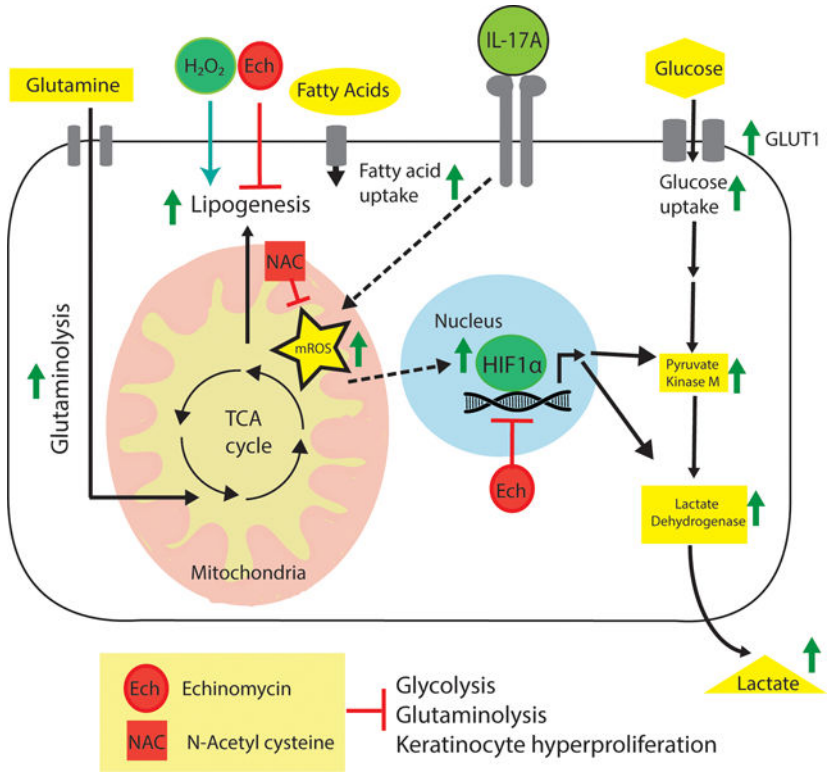

Keywords

IL-17A; Psoriasis; keratinocytes; metabolism; multiomics; cytokine; inflammation; ROS; HIF1α

INTRODUCTION

Skin is a critical site of immunological surveillance wherein immune and nonimmune cells communicate and interact through cytokine signaling mediators (1). Dysregulation of cytokine networks within and between cells can lead to pathogenesis of inflammatory cutaneous diseases. IL-17A, along with several other cytokines such as IL-9, IL-13, IL-23, and IFNγ have been implicated in the pathogenesis of several immunological diseases of the skin(2–8). In psoriasis, a prevalent skin inflammatory disorder, IL-17A is an especially abundant cytokine, and is thus of premier importance (9–12). Aberrant high expression of both IL-17A and its receptor, IL-17R (9, 13), has been linked to neutrophil infiltration, skin inflammation, and psoriatic disease progression (14, 15). IL-17A exerts paracrine effects on multiple immune cell subsets, including T-cells, neutrophils and macrophages

within psoriatic skin, and triggers secretion of multiple cytokines, including IL-6, IL-8, and TNFα, along with chemokine and angiogenic factors, thus exacerbating immune effector and homing functions and resultant skin inflammation (16, 17).

IL-17A, along with other cytokines, additionally act as crucial regulators of cellular metabolism(18) since they functionally mimic metabolic hormones (19). In this respect, they behave as sensors of nutrient fluctuations and can fine-tune adaptive immune responses accordingly (20), thus factoring heavily in the pathophysiological progression of inflammatory disorders (21–28). Such IL-17A-dependent metabolic modulation may involve a broad range of potential pathways, the specific nature of which may vary according to respective target cell type. For example, IL-17A alters lactate production and fatty acid oxidation in macrophages and decreases mitochondrial membrane potential in neutrophils through regulation of p38, Erk1/2 signaling(29, 30). Non-immune cells such as fibroblastic reticular cells of the lymph node undergo metabolic reprogramming in response to IL-17A, resulting in enhanced proliferation and survival (31). In adipocytes, IL-17A inhibits lipid and glucose metabolic pathways and suppresses adipogenesis and resultant obesity (32).

Despite extensive studies examining IL-17A-mediated immunobiological and metabolic effects, new and unexpected facets of IL-17A biology continue to emerge and numerous outstanding questions remain (33). Largely unexplored and requiring systematic dissection are IL-17A effects on major, non-immune target cells of the skin, namely keratinocytes, and its potential downstream modulation of keratinocyte-intrinsic metabolic pathways and resultant cellular functions. Regarding this, IL-17A was found to alter the urea cycle in keratinocytes overexpressing arginase-1, thus implicating an IL-17A-metabolic, pro-inflammatory feedback loop in the progression of psoriatic skin (34, 35). Additional reports have highlighted the importance of glucose and glutamine metabolism in the development of psoriasis (2, 36), now viewed as a metabolism-associated disease, in which IL-17A is believed to factor heavily in its metabolic pathophysiology. IL-17A has also been implicated in mediation of redox imbalances within inflamed skin (37–39), where elevated levels of reactive oxygen species (ROS) are thought to contribute to disease pathogenesis in both psoriasis and atopic dermatitis (40–42). Cytokines, mirroring their important roles in metabolism, may crucially regulate such redox homeostatic processes (43, 44). Indeed, we recently reported that IL-9 suppresses ROS levels in keratinocytes(25), while conversely, IL-17A increases oxidative stress in hepatocytes, peripheral monocytes and human mesenchymal stem cells (45–47). Nonetheless, IL-17A-dependent effects on downstream metabolic and redox pathways intrinsic to keratinocytes have not been comprehensively examined in either psoriasis or in any other inflammatory cutaneous disorder for that matter. Systematic evaluation of such IL-17A-triggered metabolic dysregulation and comprehensive interrogation of resultant downstream pathways directly in a major, non-immune cell type of the skin, human primary keratinocytes, is critical to comprehensive understanding of the full spectrum of IL-17A-dependent disease processes, independent from its well-established immunobiological roles (48).

Here, we systematically dissect roles of IL-17A in the metabolic reprogramming of human keratinocytes, using several independent multiomics-, systems biology-, and functional-based experimental approaches. We identified an IL-17A-dependent ROS-HIF1α axis

intrinsic to human keratinocytes involved in keratinocyte metabolic rewiring. This was marked by IL-17A-dependent elevation of mROS, HIF1α, intracellular lipids, and pro-proliferative metabolic effectors in IL-17A-treated primary keratinocytes and/or clinical skin biospecimens from patients with psoriatic disease. This study provides new mechanistic and translational insight into IL-17A and its downstream effectors in keratinocyte metabolism and psoriasis.

MATERIALS AND METHODS

Human primary and immortalized keratinocyte isolation and culture methods.

Healthy skin specimens were collected from the Plastic Surgery Department of B.Y.L. Nair Charitable Hospital, Mumbai, upon approval of the Institute Ethics Committee (IEC) of IIT Bombay and B.Y.L. Nair Charitable Hospital, Mumbai. Keratinocytes were isolated as described earlier(49, 50). Information for donors of healthy skin used for normal keratinocyte isolation (Figure 1) is shown in Table 1. In brief, sterile skin sections were dissected into smaller pieces and incubated for 16 hours at 4°C in 2.4 U of Dispase II (Roche, Mannheim, Germany). The epidermal layer was isolated by digestion with 1% Trypsin-EDTA solution (Gibco, NY, USA) for 20 min at 37°C. The epidermis was macerated, strained through a sterile gauze, and then keratinocytes obtained and cultured in serum free EpiLife media containing human keratinocyte growth supplements (Gibco, Thermo-Scientific, USA) for <5 passages. The immortalized human keratinocyte line, HaCaT (AddexBio, India), a gift from Prof. Rinti Banerjee, IIT Bombay, India, was cultured in Dulbecco's Modified Eagle's Medium (DMEM) supplemented with 10% Fetal Bovine Serum. IL-17A treatments were performed at 50 ng/ml for 24 hours except as otherwise noted, with the concentration selected based on prior studies performed by our group or others validating statistically significant effects at this concentration on HPK physiology (49),(51–54). For assays of longer duration involving HPK proliferation and viability, IL-17A concentration was maintained as above for up to 72 hours.

Validation of human primary keratinocyte purity.

Purity of keratinocyte isolates cultured from human skin were verified by flow cytometry as described(55). HPK isolates were cultured and harvested at passage three and then surface stained with PE-Cy7-conjugated anti-CD3 Ab (catalogue number: 25–0038-42, Thermofisher Scientific) and PE-conjugated anti-CD1a Ab (catalogue number: 300106, BioLegend) to rule out T cell and Langerhans cell (LCs) contamination, or intracellularly stained for the keratinocyte lineage marker using unconjugated pan-cytokeratin antibody (Catalogue number: MSM17–999-P1ABX) followed by Alexa Fluor 657-conjugated goat anti-mouse secondary Ab (catalogue number: A-21235, ThermoFisher Scientific) in the dark at room temperature. 99.1% of total cells were positive for pan-cytokeratin, with only 0.7% of cells positive for CD3, and 0.97% cells positive for CD1a, thus demonstrating high purity of keratinocyte cultures (Supplementary Figure S1a). Similar results were obtained with the positive control keratinocyte line, HaCaT, which were 99.5% positive for cytokeratin.

Sample preparation for high-throughput label-free proteomics by LC-MS/MS.

For proteomic analysis, human primary keratinocytes were treated with IL-17A (50ng/ml) for 24 hours in minimal EpiLife medium. All treatments were administered with an incubation of 24 hours at 37°C with 5% CO_2. Each of these experiments was performed with HPKs derived from 3 separate individuals (n=3 biological replicates). Sample preparation for LC-MS/MS was performed using modifications of protocols described previously (56, 57) according to the manufacturer's guidelines for Promega MS-grade Trypsin. In brief, HPKs were lysed in TRIzol reagent (Invitrogen, Carlsbad, CA) and proteins were extracted as per the manufacturer's instructions. The phenol protein fraction was separated from DNA by ethanol extraction (molecular biology grade), and protein precipitated by isopropanol. The pellet was washed with 3M Guanidium Hydrochloride solution in 95% EtOH and sonicated followed by 100% EtOH washes. Protein pellets were re-solubilized in Urea-Thiourea Buffer (8M Urea, 2M Thio-urea in Tris-Cl). A quality control check was performed using SDS-PAGE and agarose gel electrophoresis to detect any DNA contamination. The protein extract (25μg) was reduced using 10mM Dithiothreitol (Merck KGaA, Darmstadt, Germany) at 60°C for 60 min followed by alkylation with 15mM Iodoacetamide (Merck KGaA, Darmstadt, Germany) for 30 min at RT in the dark. The volume of the digestion mixture was then increased by 4x using 50mM Ammonium bicarbonate and the protein was digested using 1ug MS-grade trypsin (Promega, WI, USA) for 18 hours at 37°C. This volume of the digestion mixture was maintained constant across samples treated in the batch. The peptides thus obtained were cleaned using C18-ziptips, quantified using Scopes' method(58). Subsequently, 600 ng - 1 μg of clean peptide samples were injected into a ThermoScientific Q-Exactive Plus via an EasyNLC HPLC autosampler and C18 PepMapTM column. The instruments were set to an MS1 resolution of 70000 and an MS2 resolution of 17500. The acquisition experiments were optimized to run on 120 min and 240 min liquid chromatography gradients.

Proteomics data analysis and label-free quantification.

The MS spectra were analyzed using the Thermo-scientific mass informatics platform Proteome Discoverer Version 2.2. The common workflows for discovery proteomics were used with Mascot and SequestHT as search engines. For label-free quantification, the standard workflows by Thermo were used. Samples were normalized by peak-area based "total peptide amount". The permitted retention time (RT) shift was set to 2 min. Fragment mass tolerance was set to 0.02 Da and the precursor mass tolerance to 2ppm. The false discovery rate (FDR) was set to 0.01 (Strict). Importantly, only unique peptides were considered for peak-area based quantification. For statistical analysis of identified proteins, null hypothesis testing was performed using ANOVA (background based).

Heat map generation, functional annotation and pathway analysis of proteomics data.

A stringent protein filtering criteria was used to select for target hits used for later functional annotation and pathway analysis. This included protein hits with at least 2 unique peptides, abundance ratio *p*-value less than 0.1, and abundance ratios greater than 1.5 and less than 0.667. Filtered differentially expressed proteins were annotated for associations with biological processes using Panther server. STRING server was then used to generate

functional protein association network visualizations of filtered proteins. ClustVis server was used to generate heat maps with log2 transformed abundance ratios of the significant differentially expressed proteins.

^{1}H nuclear magnetic resonance (NMR) sample preparation, spectral acquisition and data analysis.

Keratinocyte samples were seeded in 6-well plates and treated with 50ng/ml IL-17A for 24 hours. Post 24 hours, cells were harvested, media removed, and cells were washed with PBS to remove leftover media or impurities. Cells were scraped and metabolites isolated in microfuge tubes using methanol-based extraction as described previously (25). Cells were sonicated for 6 min at 50% amplitude with 20s Pulse On-15s Pulse Off, centrifuged at 14000 rpm for 15 min, supernatant was collected, vacuum dried and stored at −80°C. Vacuum dried samples were dissolved in Phosphate Buffer (pH 7.4) containing D_2O. 10mM DSS was used as a chemical shift indicator (CSI) for referencing such that all chemical shifts were on the δH scales relative to CSI at 0. NMR experiment was performed on a Bruker spectrometer operating at 750.0 MHz for 1H NMR, at a fixed temperature of 298K, in 5 mm NMR tubes. For SIRM, vacuum dried samples were dissolved in D_2O. NMR experiments were performed on a Jeol spectrometer operating at 600.0 MHz for 1D and 13C NMR, at a fixed temperature of 298K, in 5 mm NMR tubes. 1D sample spectrums were obtained and used for identification of metabolites through analytical software. For quantitative sample profiling, spectra were processed and analysed with Bruker topspin 3.1 and Chenomx NMR suite 8.3 software. NMR spectra were initially phased in Bruker topspin 3.1 and the final baseline and spectra processing was performed using Chenomx NMR suite 8.3. Processing included baseline correction, phase correction, shim correction, CSI calibration and line broadening. Metabolites were identified using the database stored in Chenomx NMR suite 8.3 and were quantified from the comparison of the internal standard (DSS). Comparison of the spectral data obtained for each sample with the Chenomx metabolite library along with the known concentration of internal standard resulted in a list of compounds together with their respective concentrations. Metabolites identified from cytokine-treated HPK samples were run on the MetaboAnalyst 5.0, an online functional and analytical software, in which pathway and statistical analyses were performed. Metabolite concentrations were uploaded in .csv format. For normalization, sample specific normalization was performed. For statistical analysis, data was log transformed and auto scaled. For pathway analysis, only range scaling was applied.

Stable isotope-resolved metabolomics.

HPKs were cultured in 6-well plates (Merck) in EpiLife medium and stimulated with 50ng/ml IL-17A or left untreated for 24 hours. The medium was then exchanged for RPMI (ThermoFisher Scientific, Waltham, USA) containing 10 mM [U-^{13}C] glucose or 4 mM [U-^{13}C] glutamine (Cambridge Isotope Laboratories, Tewksbury, USA), with or without IL-17A for 24 hours. Cells and supernatants were collected over multiple time points and metabolites were extracted as mentioned above.

Computational analysis of metabolic flux.

A manually curated constraint-based model of human metabolic networks, Mitocore(59), was used to perform constraint-based flux balance analysis(60). MitoCore modeling comprises 324 metabolic reactions, 83 transport reactions between mitochondria and the cytosol, and 74 metabolite exchanges through the plasma membrane. This curated model was constrained for reversibility and inactivation of some reactions. Primary focus was on central metabolic networks under different physiological conditions. The model was imported into COBRApy environment(61) and optimized using the built-in Gurobi linear programming solver. For each experimental dataset and condition, we constrained uptake and secretion rates of glucose, amino acid exchange reactions, metabolites associated with central metabolic pathways based on experimental data, optimized the model using maximizing ATP (towards biomass) as the objective function, and predicted lactate and other intermediary fluxes in the central metabolic network.

Intracellular Lipid Analyses.

Adherent HaCaT (1×10^5) cells and HPKs were incubated with or without 50ng/ml IL-17A at 37°C for 24 hour, and incubated at room temperature for 20 min in the dark with either 10 μM Nile red (HaCaT) or with BODIPY (493/503) at 5 μg/ml (HPKs) or 200 ng/ml (HaCaT) (ThermoFisher Scientific). Neutral lipid content measured on a BD FACSVerse (BD Biosciences).

Lipidomics analysis.

Non-polar metabolites were extracted using methanol/chloroform protocol, were dried and used for lipidomics. At the time of LC-MS/MS injection, dried lipid samples were reconstituted in Chloroform: Methanol (1:1, v/v). Further, extracted lipids were separated on VANQUISH UHPLC system using Aquity CSH C18 column (Waters) maintained at 500C. Lipids gradient elution program comprised of mobile phase A containing ACN: H2O (60:40, v/v), with 10mM ammonium acetate and mobile phase B containing IPA: ACN (90:10, v/v), with 10mM ammonium acetate with a flow rate of 0.3ml/min. The UHPLC system was connected to Thermofisher Q - Exactive Plus mass spectrometer containing an ESI ion source. Lipids were detected in positive ion mode with a full ms scan range of 70 to 1000 m/z. The injection volume was 5μl for positive ion mode. The separated lipid species were analyzed using Lipid Search software (version 4.2.9). This study used product ion search with mass tolerance set to <5ppm, and the m-score threshold was set to 2.

Glutamine/Glutamate measurement.

HPKs were treated in the presence or absence of 50ng/ml IL-17A, NAC (10mM) and Echinomycin (2.5nM) for 24 hours. Supernatant were collected and glutamine/glutamate concentration were measured using Glutamine/Glutamate-Glo-Assay (Promega, WI, USA) according to the manufacturer protocol.

Multiple reaction monitoring (MRM) targeted proteomics assay.

HPKs were treated with IL-17A (50ng/ml) and/or echinomycin (2.5nM) for 24 hours. Proteins were then extracted in urea (6M) and thio-urea (2M) buffer made in Tris-Cl.

25μg protein was then treated with dithiothreitol (DTT) and iodoacetamide (IAA) and digested in MS-grade trypsin (Promega, WI, USA). Peptides were desalted in C-18 silica based material, quantified. All transitions for unique peptides with 0 missed cleavages (precursor ion +2 charge, and product ion +1 charge) as predicted by the Skyline™ Daily software (Ver 22.2.1) were monitored. We first refined this list on a pool of IL-17A treated samples. 6 peptides of LDH-A (LVIITAGAR, NVNIFK, FIIPNVVK, QVVESAYEVIK, VTLTSEEEAR, SADTLWGIQK) and 8 peptides of PKM (LDIDSPPITAR, ITLDNAYMEK IYVDDGLISLQVK, GADFLVTEVENGGSLGSK, FGVEQDVDMVFASFIR, AGKPVICATQMLESMIK, LAPITSDPTEATAVGAVEASFK, and VNFAMNVGK) were finalized. 3 bio-replicates of each condition were used for the MRM experiment and results acquired were analysed on Skyline™ Daily. For the MRM sample runs, around 1.6 ug of peptides were injected onto Hypersil gold C18 column with an Ultimate 3000 UHPLC system. A binary buffer system (Buffer A = 0.1% Formic acid in water and Buffer B = 0.1% Formic acid in Acetonitrile) allowed for the separation of peptides that were fed directly into the Thermo TSQ Altis system for data acquisition. All the data and results have been made available at the URL: https://panoramaweb.org/IL17A-keras-glycolysis.url.

Glucose Uptake and Lactate Quantification.

Cells were stimulated with IL-17A at 10, 25 or 50 ng/ml for 24 h. Media was removed, cells were washed in PBS, 2-NBDG (10μM) was added in glucose-free RPMI media (200 μl), and cells were incubated for 30 min at 37°C. Finally, media was removed, cells were washed, and data was acquired on a BD FACSVerse (BD Biosciences, NJ, USA).

HPKs were treated in the presence or absence of 50ng/ml IL-17A for 24 hours in EpiLife medium. Cell-free supernatants were incubated in lactate assay buffer (NAD+ substrate plus 1 U/ml Lactate Dehydrogenase in Tris-Glycine-Hydrazine, pH 9.0) for one hour at 37°C. Absorption at 340 nm was read to detect NADH.

Insulin was used as a positive control in the assays above assessing lactate production and glucose uptake as described (62). Cells were incubated with insulin (150nM) or IL-17A (50ng/ml), in DMEM without glucose (catalogue no. D5030). For glucose uptake assays, media was removed post-incubation and replaced with fresh medium containing 2-NBDG (10μM), IL-17A and/or Insulin, for 30 min at 37°C, media removed, cells washed, and data acquired on a BD FACSVerse (BD Biosciences, NJ, USA). For assays assessing lactate production, cells were incubated with insulin and/or IL-17A in low glucose (10mM) DMEM for 24 h. Supernatants were collected and lactate levels quantified as described above.

Fatty Acid Uptake Assay.

Palmitic acid uptake was measured by incubating cells with 100 nM BODIPY FL C 16 (ThermoFisher Scientific) for 30 min at 37ºC in FBS-free medium. Cells were washed in four volumes of ice-cold PBS containing 2% FBS to stop the reaction. Finally, cells were trypsinized, collected, washed twice in PBS, and then subjected to flow cytometric analysis. Results are reported as the geometric mean fluorescence intensity.

Cell viability and proliferation analyses.

HaCaT and HPKs (0.1 million/ml) were suspended in DMEM, 10% FBS, 1% penicillin/streptomycin or complete Epilife medium and seeded into 24-well plates. Cells were pre-treated with 3uM NAC (for 1 hour in respective wells), or 2.5nM echinomycin or metabolites (10uM Glucose, 4uM Glutamine, 2uM Sodium Pyruvate and 2uM Malic acid). Cells were then cultured for 24 h or 72 h in the presence or absence of IL-17A (50ng/ml). Post-incubation, cells were harvested and stained for trypan blue, and cell viability was calculated by dividing the number of live cells by total cell number.

Flow Cytometric staining of GLUT1 and HIF1α.

HPKs were stimulated with IL-17A (50 ng/ml) and/or H_2O_2 (50 μmol/L) and/or pre-treated with NAC for 4 hour. Cells were washed once in FACS buffer (2% FBS in PBS) at 4°C and then incubated with the Fixation-Permeabilizing Solution (ThermoFisher Scientific) at room temperature for 40 min. Fixed HPKs were stained with unconjugated rabbit anti-human HIF1α Ab (PA1–16601) or GLUT1 (MA5–31960), ThermoFisher Scientific), then with Alexa Fluor 488-conjugated goat anti-rabbit Ab (A-11008, ThermoFisher Scientific) and acquired on a BD FACSVerse flow cytometer (BD Biosciences).

Western Blot Analyses.

HaCaT cell cultures at <60% confluence were treated with IL-17A (50ng/ml) in incomplete DMEM media for 8 h. Cells treated with EGF (20ng/ml) and $CoCl_2$ were used as positive controls. Cells were lysed by sonication at 4°C in RIPA buffer (Sigma-Aldrich, Germany) supplemented with 2mM $CoCl_2$ and a protease and phosphatase inhibitor cocktail (Sigma-Aldrich, Germany). Lysates were quantified by the BCA assay (Pierce, ThermoFisher scientific), and 35–50 μg of protein was resolved by SDS-PAGE at 60–90V. Proteins were transferred to PVDF membranes using a Trans-Blot Semi-Dry Transfer Cell (Bio-Rad, Hercules, CA, USA), blocked in 7.5% non-fat dry milk (Himedia, India) dissolved in TBS/0.25% Tween-20 (Merck, Germany), and then probed with rabbit anti-human HIF1α and mouse anti-human GLUL (PA1–16601 and MA-527749, ThermoFisher Scientific, Waltham, USA) or anti-actin primary Abs (PA1–183, ThermoFisher Scientific, Waltham, USA) in blocking buffer. Membranes were washed in TBS/0.25% Tween-20, incubated with HRP-conjugated goat anti-rabbit secondary Ab (G-21234, ThermoFisher Scientific, Waltham, USA), and developed with ECL Chemiluminescent Substrate (Bio-Rad, California, USA) using the iBright FL1500 Imaging System (ThermoFisher Scientific, Waltham, USA). Images were analyzed by ImageJ software by normalizing mean grey value band intensities of HIF1α (100–120 kDa) to corresponding actin (42kDa) bands.

Apoptosis Assay.

HPKs were seeded in complete EpiLife media at 1×10^5 cells/well in 12-well plates for 24 hour. Media was replaced with minimal Epilife containing IL-17A with or without echinomycin (Sigma-Aldrich, Germany) for 48 h, with one replenishment of IL-17A halfway through. Similarly, for glutamine synthetase related apoptosis experiments, HaCaT cells were cultured in complete DMEM for 24 hours. The media was then replaced with glutamine deficient RPMI with or without the GS inhibitor, methionine sulfoximine (MSO)

(Sigma-Aldrich, Germany) over 36 hours, with one replenishment of IL-17A at the 24-hour mark. In both cases, cells were, trypsinized, harvested, washed in PBS, and stained with PE-conjugated Annexin V followed by 7-AAD (Annexin-V Apoptosis Detection Kit, ThermoFisher Scientific). Flow cytometric analyses for early- and late-stage apoptosis and necrosis were performed on a BD FACSVerse (BD Biosciences).

Oxidative Stress Evaluation.

HPKs were seeded into 12-well plates and treated with or without 50ng/ml IL-17A indicated for 4 h or 24 h. Cells were washed with PBS and stained with 1 μM 2,7-dichlorodihydrofluorescein diacetate (H2DCFDA, Sigma-Aldrich, Germany) in 1ml PBS or 5 μM MitoSOX Red (ThermoFisher Scientific) in 200 μl PBS for 20 min at 37°C to measure cellular and mitochondrial ROS levels, respectively(63). Data was acquired on a BD FACSVerse (BD Biosciences).

Immunofluorescence Staining of Skin Biospecimens.

Information for donors of healthy and psoriatic skin biopsies is shown in Table 1. Skin biospecimens obtained from psoriatic patients and healthy individuals were snap-frozen in isopentane and stored in liquid nitrogen. Biopsies were embedded in OCT solution (ThermoFisher Scientific, Waltham, USA), cryosectioned at −25°C, and seven micrometer thick sections were immobilized on silane-coated slides (BioMarq, India) and stored at −80°C or 4°C until needed for immunofluorescence and ROS studies, respectively. For staining of HIF1α, GLUL and Ki-67, cryosections were thawed at room temperature, fixed in 4% paraformaldehyde and blocked in 2% BSA/PBS (5% BSA/PBS for Ki-67). Anti-HIF1α Antibody, anti-GLUL antibody and anti-Ki-67-FITC conjugated antibody (PA1–16601, MA-527749 and 11–5698-82 respectively, ThermoFisher Scientific), in 2% BSA, 0.3% Triton-X100, PBS was incubated overnight (2 hour at RT for Ki-67), washed in PBS, and incubated 2 h with Alexa Fluor 488-conjugated goat anti-rabbit secondary Ab (A11008, ThermoFisher Scientific) in the dark at room temperature. Sections were counterstained with 4′,6-diamidino-2-phenylindole (DAPI), dried, mounted with ProLong Gold Antifade Mountant (ThermoFisher Scientific), and imaged using an EVOS M7000 Imaging System (ThermoFisher Scientific). ImageJ software was used to measure the integrated density of HIF1α staining, which was then normalized across sections to unit length of skin. For staining of ROS, sections were washed with warm PBS, incubated with 5μM MitoSOX (510/580) for 20 min at 37°C in dark to stain mROS, stained with DAPI (5 μg/ml) for 5 min in the dark at room temperature, washed in PBS and mounted with DPX solution. Sections were visualised with an LSM 780 microscope under 10x and 40x magnification using ZEN Blacksoftware, and the mean fluorescence intensity of images were analyzed with ImageJ.

For staining of lipids, cryosections were fixed in 4% paraformaldehyde for 5 min at RT, incubated with 50 μg/ml BODIPY in DMSO (493/503) for 30 min in the dark at room temperature, and stained with DAPI (5 μg/ml) for 5 min in the dark at room temperature. Slides were washed in PBS, mounted with DPX solution (Dibutylphthalate Polystyrene Xylene, Sigma-Aldrich, Germany), and imaged with an LSM 780 microscope (Zeiss, Oberkochen, Germany) under 10x magnification using ZEN Black software (Zeiss, Oberkochen, Germany). Mean fluorescence image intensities were analyzed using ImageJ.

Statistics.

Proteomic analysis abundance ratio p-values were calculated using background-based ANOVA (Figures 1a, Supplemental data). *P*-values were calculated by Student's paired or unpaired *t*-test (Figures 2, 3, 4, 5, 6) as indicated. *P*-values < 0.001, < 0.01, and < 0.05 are represented as ***, **, and *, respectively.

Study Approval.

All studies involving human specimens were approved by the Institute Ethics Committee (IEC, Approval ID: SVD/47) of IIT Bombay and B.Y.L. Nair Charitable Hospital, Mumbai. Written informed consent was obtained from all subjects and all studies were conducted in accordance with the Declaration of Helsinki.

RESULTS

Tandem LC-MS high-throughput quantitative proteomics reveals modulation of metabolic pathways in keratinocytes by IL-17A

IL-17A-stimulated HPKs ($n = 5$) were subjected to high-throughput label-free quantitative LC-MS/MS. The heat map depicts 401 differentially expressed proteins (≥1.5-fold change) out of 2111 total proteins detected with high confidence (Supplemental Data), of which the top 100 are listed by name ($n = 5$, $p \leq 0.1$, Supplementary Figure S1b). As expected, established IL-17A targets in psoriatic and inflammatory diseases, including IL-36, members of the small proline-rich (SPRR) family (SPRR2A and SPRR2D), and S100 (S100A7, A8, and A9) family proteins were upregulated by IL-17A. Notably, PantherDB-based functional relationship analysis revealed that ~31% of all differentially expressed proteins were associated with cellular metabolic processes (Figure 1a). Consistently, six major metabolic clusters downstream of IL-17A signaling were identified using STRING protein association network studies, including the TCA cycle, pyruvate, lipid, and primary metabolic processes, precursor metabolites and energy mediators (Supplementary Figure S1c).

IL-17A significantly altered levels of key proteins involved in carbohydrate and glutamine metabolism, such as enzymes involved in glycolysis (pyruvate kinase, lactate dehydrogenase A), lactate transport (monocarboxylate transporter SLC16A1), TCA cycle (isocitrate dehydrogenase isoforms G and B, and succinate CoA ligase) and glutamine synthesis (Glutamine synthetase, GLUL) (Figure 1b). IL-17A treatment also upregulated the biosynthesis of lipids, particularly cholesterol and sphingolipids, in HPKs (Figure 1c). Together, the proteomics analyses support IL-17A as a crucial regulator of carbohydrate, glutamine and lipid metabolic pathways in human primary keratinocytes.

IL-17A regulates metabolic flux in keratinocytes as revealed by NMR-based metabolic profiling and systems biology simulations

We next investigated the effects of IL-17A on metabolic profile and flux of defined pathways in HPKs using ^{1}H-NMR metabolic profiling. Metabolites were extracted from IL-17A-treated HPKs, chemically identified, and then quantified using ^{1}H-NMR spectroscopy (Chenomx NMR Suite 8.3) (Supplemental Data). The heat map in Supplementary Figure S2a depicts top 75 metabolites that were dysregulated in IL-17A-

treated keratinocytes. Pathway analysis using MetaboAnalyst 5.0 revealed alterations in TCA cycle and pyruvate metabolism (Figure 1d). IL-17A treatment significantly dysregulated ($p < 0.05$) concentrations of metabolites such as glucose, malate, sarcosine, and glutathione, involved in carbohydrate metabolism (Figure 1e).

To map the global effects of IL-17A on central carbohydrate metabolism in HPKs, we inserted the flux values of differentially regulated metabolites (Supplemental Data, constraints for mitocore) into MitoCore, a systems biology tool used for simulating metabolic changes (59). The resultant metabolic model (Figure 1f) revealed IL-17A-mediated increases in glycolysis, glutamine uptake and glutaminolysis pathways, as depicted by upward-pointing arrows. The simulation further predicted increased flux toward pyruvate from both glucose and glutamine sources, which is then redirected toward lactate production. Increased flux of malate to pyruvate was also predicted, along with resultant elevation in lipid metabolism. In summary, the metabolic profiling and multiomics simulation studies indicated that IL-17A potentiates metabolic reprogramming in HPKs by markedly increasing overall nutrient intake, thus leading to enhanced glycolysis, glutaminolysis, and lipid accumulation.

Stable isotope-resolved metabolomics and biochemical assays confirm IL-17A-mediated upregulation of glycolysis and glutamine metabolism in keratinocytes

We next experimentally validated the metabolic profiling results and simulation predictions by employing Stable Isotope-Resolved Metabolomics (SIRM) to directly quantify IL-17A-mediated nutrient uptake and metabolite production in *ex vivo* keratinocyte culture systems. Specifically, SIRM was used to trace the fate of ^{13}C-labeled glucose ([U-$^{13}C_6$]-Glc) in IL-17A-treated HPK cultures (Figure 2a). Briefly, control and IL-17A-treated HPKs (post-24 hour stimulation) were cultured in RPMI medium devoid of glucose and then supplemented with U-^{13}C-labeled glucose. Culture supernatants were collected at defined time points, and lactate production was quantified (Figure 2b). 13C NMR spectra depict ^{13}C-glucose (Figure 2c) and ^{13}C-lactate amounts (Figure 2d), respectively, in HPK supernatants 24 hours after the addition of ^{13}C-glucose. NMR-based 13C and 1H investigations revealed a significant increase in lactate production (Figure 2e) at 4 and 8 hours in IL-17A-treated HPKs as compared to untreated control cells. Moreover, glucose uptake by HPKs increased with elevating concentrations of IL-17A (Figure 2f) or positive control insulin (150nM, Supplementary Figure S2b), thus corroborating the results above supporting an IL-17A-stimulated enhancement of glycolytic flux. In fact, IL-17A stimulation induced greater uptake of glucose in HPKs in comparison to insulin, thereby affirming IL-17A as a potent regulator of keratinocyte metabolism.

Next, we employed SIRM to trace the fate of uniformly ^{13}C-labeled glutamine ([U-$^{13}C_6$]-Gln) in IL-17A-treated HPKs (Figure 3a). As described above, both IL-17A-stimulated and untreated control HPKs were cultured in RPMI medium without glutamine and then supplemented with 4 mM U-^{13}C glutamine ([U-$^{13}C_5$]-Gln); the culture supernatants were collected at different time points, and lactate was quantified (Figure 3b). SIRM analysis revealed a significant increase in glutamine-derived ^{13}C-lactate production at 8 and 12 hours (Figure 3c). Moreover, there was a decrease in glutamine (p value: 0.06) and concurrent

increase in glutamate concentration in the supernatants of IL-17A-treated keratinocytes, indicative of increased glutamine consumption (Figure 3d). Thus, IL-17A promoted the utilization of glutamine as an alternative, non-glucose carbon source for anaplerosis to enhance energy production in keratinocytes.

We employed biochemical assays to further confirm the multiomics results above. Indeed, IL-17A treatment significantly augmented extracellular levels of lactate, assayed biochemically, in supernatants of HPK cultures (Figure 3e). Treatment with insulin, an established positive control and known physiologic mediator of glycolysis, also significantly increased keratinocyte-intrinsic lactate production (Supplementary Figures S2c). The production of lactate varied based on the presence or absence of glucose (10 mM) and glutamine (4 mM) in the medium, wherein lactate levels were ~1.6-fold higher in glucose versus glutamine supplemented media (Figure 3f). These results thus corroborate the IL-17A-dependent triggering of glycolysis predicted above, including the increased reliance on glucose over glutamine as a substrate for lactate production.

Along with glutaminolysis, we also studied the mechanism for endogenous glutamine production affected by IL-17A treatment. As shown in figure 1b, glutamine synthetase (GLUL) was found to be upregulated in keratinocytes. We found that the expression of glutamine synthetase is dependent on the levels of glutamine availability (Figure 3g) with a higher expression observed in glutamine scarcity. As these metabolites serve a crucial role in keratinocyte physiology and functions, we wanted to explore their role in HPK proliferation. IL-17A-treated HPKs were cultured in the presence of various metabolites. We observed that glucose, glutamine and pyruvate were required for proliferation of keratinocytes (Figure 3h). Interestingly, we observed glutamine to be extremely critical for HPKs enhanced proliferation. To underscore the reliance of IL-17A stimulated keratinocytes on glutamine, we inhibited the activity of GLUL using methionine sulfoximine (MSO) in glutamine deficient medium. We found IL-17A stimulated cells to undergo significantly higher apoptosis than untreated cells (Figure 3i). Moreover, psoriasis biopsies probed for GLUL showed enhanced expression of this enzyme as compared to healthy biopsies, highlighting the importance of glutamine in disease progression (Supplementary Figure S2d).

IL-17A promotes the uptake and accumulation of lipids in human keratinocytes

Considering that MitoCore modeling and proteomic analyses showed marked increases in lipid biosynthetic processes and activation of sphingolipid metabolism, we performed lipidomic analysis to compare the lipidome of IL-17A-treated with untreated HPKs. We present here a comprehensive lipid profile revealing increased polar and neutral lipids in IL-17A-treated HPKs. Specifically, IL-17A treatment significantly increased concentration of ceramide, sphingomyelin, and triglyceride lipid classes in primary keratinocytes (Figure 4a-c, Supplemental Data). To validate the lipidomics data, we quantified the lipid content of keratinocytes using BODIPY and Nile Red fluorescent staining. In agreement with our prior results, IL-17A treatment significantly increased lipid content as indicated by BODIPY staining in both HPKs (Figure 4d) and HaCaT cells (Figure 4e) and by Nile Red staining (Supplementary Figure S2e). As expected, intracellular lipid content was also markedly

elevated by treatment with the positive control, oleic acid-conjugated albumin, which is an established stimulator of lipid accumulation(64). Next, we investigated the mechanism of IL-17A-mediated increase in lipid content. Notably, IL-17A significantly promoted lipid uptake by HPKs and HaCaT cells, as determined using BODIPY FL C16 staining (Figures 4f and 4g, respectively). To validate these results *in vivo*, we measured intracellular lipid levels in both healthy and psoriatic skin biospecimens. Significantly enhanced intracellular lipid pools were indeed confirmed in skin biospecimens obtained from psoriasis versus healthy control patients based on BODIPY (493/503) staining (Figure 4h). Collectively, these results support the notion that IL-17A promotes increased levels of intracellular lipid pools in human keratinocytes.

An IL-17A-mediated ROS–HIF1α axis regulates metabolic reprogramming in human keratinocytes

Given that HIF1α is a known transcriptional regulator of IL-17A-dependent glycolysis, and a metabolic effector molecule, we assessed whether HIF1α might be a downstream target of IL-17A signaling in HPKs. Notably, IL-17A increased HIF1α levels in human keratinocytes (Figure 5a). Because IL-17A induced HIF1α, an established sensor and target of oxygen and reactive oxygen species (ROS), we examined the effects of IL-17A on oxidative stress and ROS levels in HPKs. IL-17A significantly increased both cytosolic (c) and mitochondrial (m) ROS levels in HPKs (Figure 5b). Moreover, IL-17A-mediated changes in ROS levels were reduced by addition of the antioxidant, N-acetyl cysteine (NAC) (Figure 5b). Given that ROS is a known agonist of HIF1α (4), we further assessed whether ROS stimulated expression of HIF1α in IL-17A-treated keratinocytes. As predicted, induction of ROS by either IL-17A or H_2O_2 (50 μmol/L) significantly increased the expression of HIF1α, whereas inhibition of ROS by NAC reduced it (Figure 5c).

To determine if ROS-HIF1α axis was functionally involved in the IL-17A-mediated metabolic reprogramming, we employed echinomycin, a peptide antagonist of HIF1α (65) and NAC, an antioxidant. We performed targeted mass spectrometry using multiple reaction monitoring (MRM) to investigate the effector proteins involved in IL-17A-mediated metabolic reprogramming. Expression of Lactate Dehydrogenase A and Pyruvate Kinase (key metabolic downstream gene targets of HIF1α) (66), were found to be significantly upregulated by IL-17A, which were subsequently reduced by echinomycin (Figure 5d-e, Supplementary Figure S3). Further, IL-17A increased expression of the glucose transporter protein type 1 (GLUT1) in HPKs, which was reversed upon treatment with echinomycin or NAC (Figure 5f). Echinomycin and NAC blocked IL-17A-induced lactate production (Figure 5g-h), lipid synthesis (Figure 5i) and glutamine consumption in HPKs (Figure 5k). Consistently, induction of ROS production by H_2O_2 (50 μmol/L) further increased intracellular levels of lipids in HPKs (Figure 5j), highlighting ROS as a crucial metabolic regulator of the IL-17A–HIF1α axis. Together, these results reveal a ROS-HIF1α axis in the metabolic reprogramming of keratinocytes downstream of and specific to IL-17A (Figure 5l).

IL-17A drives HIF1α- and ROS-mediated hyperproliferation in psoriasis

Because IL-17A potently triggered energy metabolism via ROS–HIF1α as evidenced by significant induction of carbohydrate, glutamine, and lipid metabolic pathways, we examined the functional involvement of HIF1α in the IL-17A-driven proliferation of keratinocytes (Supplementary Figure S3c). Inhibition of HIF1α with echinomycin markedly blocked IL-17A-mediated survival (Figure 6a-b) and viability (Figure 6c) of HPKs as well as of HaCaT cells (Supplementary Figure S3d). Moreover, immunofluorescence staining revealed increased levels of HIF1α in the epidermis of psoriatic skin as compared with that in biopsies from healthy control individuals (Figure 6d).

Given that ROS is an established marker of cellular proliferation(67) and is involved in HIF1α activation, we next examined whether the observed increase in ROS promoted the growth of keratinocytes. Indeed, IL-17A stimulation significantly enhanced, while inhibition of ROS by NAC reduced, proliferation of keratinocytes (HPKs, Figure 6e; HaCaT, Supplementary Figure S3e). Consistently, mROS levels were significantly increased in the epidermis of proliferating psoriatic skin specimens compared with those in healthy control samples (Figure 6f). Moreover, IL-17A increased expression of the pro-proliferative marker, Ki-67, in human keratinocytes which was reduced by the inhibitory effects of echinomycin and NAC (Figure 6g). The results were consistent with immunofluorescence-based staining revealing co-expression of mROS and Ki-67 in Psoriatic skin (Figure 6h), thus reflecting involvement of mROS in cell proliferation. Together, these data reveal an IL-17A–triggered ROS–HIF1α axis operative in the metabolic reprogramming and hyperproliferation of human keratinocytes during IL-17A-mediated skin inflammation.

DISCUSSION

The inflamed psoriatic skin microenvironment contains numerous cytokine effectors, including IL-17A, along with IL-23, IL-36, IFNγ, and TNF-α, among others. These signaling mediators trigger pleiotropic effects on multiple cell types leading to disease progression. Despite the presence of several distinct cytokines, IL-17A factors critically in psoriatic disease etiopathology(68) as evidenced by the fact that administration of Secukinumab, a blocking antibody targeting IL-17A, results in rapid improvement in clinical, histopathological, and molecular indications of psoriasis (69). Furthermore, numerous murine models of psoriasis emphasize the crucial importance of the IL-17A pathway in experimental psoriasis. As IL-17A represents a premier cytokine in the pathogenesis of psoriasis (68), we systematically examined IL-17A-mediated metabolic reprogramming pathways intrinsic to keratinocytes using several independent methodologies, including high-throughput shotgun and targeted mass spectrometry-based proteomics, lipidomics, SIRM, NMR spectroscopy, flow cytometry, and immunofluorescence in both primary cultures and clinical tissues of patients with psoriasis. We identified IL-17A-mediated increases in glycolysis, glutaminolysis and lipid accumulation in HPKs, and downstream HIF1α and ROS in regulation of these metabolic rewiring processes in keratinocytes in psoriasis. Increased expression of ROS and HIF1α were detected in psoriasis lesional skin. Pharmacological inhibition of the ROS–HIF1α axis reversed IL-17A-driven pro-proliferative metabolism and keratinocyte pathophysiology.

Together, these results provide new mechanistic insights into IL-17A-dependent metabolic reprogramming of a major, non-immune cell type within human skin, the keratinocyte. They also identify ROS and HIF1α as promising downstream therapeutic targets for reversing IL-17A-driven metabolic sequelae and hyperproliferation in inflamed skin in psoriasis.

The IL-17A-triggered upregulation of glycolytic enzymes coincided with enhanced glucose flux into keratinocytes, as validated by glucose uptake assays, and was consistent with our systems-based model predicting increased glycolytic flux, glutaminolysis, and resultant enhancement of lactate production and increased lipid synthesis. SIRM was employed to confirm these algorithmic predictions, wherein ^{13}C-labeled glucose and glutamine were incorporated into HPK culture medium and were found to contribute to increased production of ^{13}C-labeled lactate, with glucose being the predominant source. In accordance with our findings, increased glycolytic activity and lactic acid levels have been previously reported in psoriasis patients (70–72). A recent study by Konieczny et al. also showed that IL-17A-mediated increased glycolysis is associated with wound healing in the mouse epidermis(73). It has been previously noted that targeting glucose uptake and/or glycolytic flux via inhibition of GLUT1 and CD147 suppressed imiquimod (IMQ)-induced psoriasis-like inflammation in mice, thus highlighting glucose metabolism in psoriasis pathogenesis(36, 74–76). IL-17A-induced glycolysis and glutaminolysis demonstrated in this study potentially mirrors the metabolic alterations of psoriasis, in which high glucose and glutamine uptake are critical for survival of psoriatic cells (36, 77). Our results corroborate these findings by underscoring glutamine, in comparison to other metabolites, as particularly critical in IL-17A-driven HPK proliferation. Glutamine is indispensable for DNA and protein synthesis and cell proliferation (78), thus rationalizing therapeutic strategies to block exogenous glutamine uptake to reduce psoriatic lesional growth and survival as reported (79). In further support, Wang et al. uncovered immuno-metabolic crosstalk between the miR-31–5p micro-RNA, which is highly expressed in keratinocytes of psoriatic skin, and glutamine metabolism. MicroRNA-31–5p promoted Th17 cell differentiation pathways and also increased glutamine metabolism and corresponding pro-survival and pro-proliferative functions(80). These findings consistent with our results of IL-17A-dependent increases in keratinocyte glutaminolysis. Enhanced glutaminolysis in IL-17A-treated HPKs led to scarcity of exogenous glutamine, thereby inducing glutamine synthetase enzyme expression, possibly through a glutamine concentration dependent mechanism (81). Inhibition of glutamine synthetase resulted in keratinocyte cell death in cultures with exogenous glutamine scarcity, thus, highlighting this enzyme as a key regulator of glutamine accessibility to hyperproliferating keratinocytes. Psoriatic biopsies showed similarly increased expression of glutamine synthetase, as previously reported(82). Thus, metabolic overreliance on anaerobic glycolysis and glutamine addiction could be exploited as potential therapeutic targets of the IL-17A axis.

In addition to our analyses of IL-17A-dependent regulation of central carbohydrate metabolism, we analyzed its role in lipid biosynthesis, given the crucial role of lipid reservoirs as sources of cellular energy and membrane building blocks, and in proliferation and inflammation (83, 84). Proteomics and systems biology data revealed IL-17A-mediated alterations of lipid metabolism as IL-17A-treated keratinocytes showed enhanced activation of the lipogenesis pathway involving upregulation of multiple enzymatic regulators of

cholesterol and sphingolipid biosynthesis. Lipidomics analyses uncovered increased levels of sphingolipids (ceramides, sphingomyelin) and triglycerides in IL-17A-treated HPKs, as corroborated by biochemical functional assays demonstrating enhanced intracellular lipid content and fatty acid uptake by IL-17A-stimulated HPKs. Other groups have reported IL-17A-mediated rewiring of lipid metabolism in additional cell types, including fibroblasts, dendritic cells and hepatocytes, underscoring IL-17A as a modulator of lipid metabolism across diverse cell lineages(9, 31, 85, 86). Our results identifying increased lipid accumulation specifically in keratinocytes in response to IL-17A might thus partly explain the abnormal lipid metabolism associated with psoriasis (87). Indeed, we detected increased intracellular lipid accumulation in the epidermis of psoriasis patients as compared to healthy individuals. Likewise, multiple studies report increasing risk of psoriasis with increasing lipoprotein, glycerophospholipid and serum lipid concentrations (88–91). In fact, cholesterol crucially regulates IL-17A signaling in psoriasis (92), again highlighting the interplay between IL-17A and metabolic dysregulation.

We identified the oxygen-sensitive transcription factor, HIF1α, as a key regulator of IL-17A-driven metabolic reprogramming in keratinocytes. HIF1α level can be controlled by multiple mechanisms, of which the most prominently described involves its upregulation under hypoxic conditions (93). HIF1α expression can still be induced under scenarios of normal oxygen level, termed normoxic, by agonists such as Insulin-like growth factor 1 (IGF1) through an oxygen-independent mechanism termed pseudohypoxia(94, 95). We found significant upregulation of HIF1α in both HPKs and HaCaT cells in response to IL-17A treatment even under normal oxygen conditions, coinciding with elevated glycolysis, glutaminolysis, lipid accumulation, and proliferation. Inhibition of HIF1α with echinomycin reduced extracellular lactate levels, intracellular neutral lipid amount, glutamine uptake, and HPK proliferation, thereby highlighting HIF1α as a critical downstream effector of the IL-17A-driven metabolic rewiring of human keratinocytes. Unlike near-normoxic conditions found in cell culture incubators of 20% oxygen, a state of hypoxia has been reported in the human epidermis *in vivo*(96). Such reduced oxygen levels coincide with elevation of HIF1α expression in the skin. It is hence plausible that IL-17A signaling, which we found to induce downstream hypoxia-associated pathways such as HIF1α may thus exacerbate pre-existing, baseline hypoxic effects(96). Additional studies have also found increased HIF1α expression in psoriatic lesions and serum of patients with psoriasis (97–100) and further demonstrate its ability to regulate GLUT1 expression and keratinocyte proliferation in psoriasis (101). Though our results regarding IL-17A-dependent effects are valid under the conditions tested, different dosages and/or time points might yield different results. Moreover, the contribution of other cytokine mediators to these keratinocyte-intrinsic processes within inflamed skin requires further investigation.

Our data identifying an IL-17A–HIF1α axis in regulation of keratinocyte metabolism, prompted us to investigate ROS as a potentially critical agonist of this pathway, particularly in light of prior reports demonstrating ROS-mediated regulation of HIF1α(102, 103). However, whereas these studies involved cancer cells, to our knowledge, there are no reports regarding IL-17A-mediated ROS-dependent regulation of HIF1α in primary human keratinocytes. Cellular and mitochondrial ROS levels were increased in HPKs and HaCaT cells in response to IL-17A. Our metabolomics-based studies further revealed

decreased levels of the antioxidant, glutathione, a key regulator of redox homeostasis (Figure 1e). Interestingly, induction of ROS upregulated HIF1α expression, subsequent production of lactate and intracellular lipids, and keratinocyte hyperproliferation. In agreement, we detected increased expression of mROS and intracellular lipids in psoriatic skin biopsies, consistent with a recent report identifying overproduction of ROS and lipid mediators in patient psoriasis samples(42). We also found co-expression of mROS with Ki-67 in epidermal tissue from psoriatic patients, pointing to an association with keratinocyte hyperproliferation. Redox homeostasis is functionally important in both healthy and tumor cells (Supplementary Figure S3f), as in normal cells elevated ROS can trigger pro-proliferative signaling to promote inflammation, while conversely inducing cytotoxicity in malignant cells. Such IL-17A-driven oxidative stress and hyperproliferation can be reduced in psoriatic skin via topical or oral administration of glutathione, which has proven clinically beneficial for disease prevention and recurrence(104). Additional ROS-associated pathway antagonists are currently under evaluation to alleviate psoriatic skin inflammation(105), including inhibitors designed to reduce excess ROS levels by targeting NADPH oxidase and the Nav1.8 sodium channel(106–108). This study provides new mechanistic and translational insight into IL-17A-dependent downstream pathways in keratinocyte metabolism and function by leveraging systematic metabolomics-based approaches. We uncover a heretofore undescribed IL-17A–ROS–HIF1α axis intrinsic to keratinocytes that modulates downstream metabolic processes and proliferation, and associates with psoriatic disease pathology. By considering the keratinocyte as both a non-immune target cell of IL-17A, and one that undergoes metabolic rewiring in response to IL-17A exposure, this work adds to the growing body of knowledge into IL-17A biological functions in inflammatory settings. It also lays the groundwork for future studies aimed at evaluating drugs targeting the IL-17A-axis in keratinocytes, further validating the *in vivo* significance of these results, and dissecting roles of additional cytokine networks and metabolic activities potentially operative in psoriasis.

Supplementary Material

Refer to Web version on PubMed Central for supplementary material.

ACKNOWLEDGEMENTS

We thank central facilities (SAIF MS and NMR) at IIT Bombay. We are grateful for the support from Manali Jadhav, Meenal Jadhav, Nutan M. Agadi, Eshant Bhatia for help in MS and NMR instrumentation and sample preparation. We also thank the patient volunteers who participated in this study and their family members and the medical staff at B.Y.L. Nair Charitable Hospital.

FOOTNOTE/FUNDING SOURCES

This work was supported by a Department of Science and Technology (DST) grant RD/0119-DST0000-10 (to RP), an Indian Council of Medical Research (ICMR) grant RD/0119-ICMR000-001 (to RP), an IIT Bombay intramural fund (to RP), a Department of Biotechnology (DBT) student fellowship (to SM), and NIH/NCI grants R01CA247957 and R01CA258637 (to SRB).

DATA AVAILABILITY

The datasets generated and/or analyzed during the current study are available from the corresponding authors on reasonable request. Raw data for shotgun proteomics experiments can be found as doi:10.25345/C5G15TF96 in MassIVE, and as PXD035995 on ProteomeXchange, the open-source online data public repositories for mass spectrometric data. [dataset license: CC0 1.0 Universal (CC0 1.0)]. Targeted MS data can be found at the URL: https://panoramaweb.org/IL17A-keras-glycolysis.url.

REFERENCES

1. Nguyen AV, and Soulika AM 2019. The Dynamics of the Skin's Immune System. International journal of molecular sciences 20:1811. [PubMed: 31013709]
2. Xia X, Cao G, Sun G, Zhu L, Tian Y, Song Y, Guo C, Wang X, Zhong J, Zhou W, Li P, Zhang H, Hao J, Li Z, Deng L, Yin Z, and Gao Y. 2020. GLS1-mediated glutaminolysis unbridled by MALT1 protease promotes psoriasis pathogenesis. The Journal of clinical investigation 130: 5180–5196. [PubMed: 32831293]
3. Noelle RJ, and Nowak EC 2010. Cellular sources and immune functions of interleukin-9. Nature reviews. Immunology 10: 683–687.
4. Bonello S, Zahringer C, BelAiba RS, Djordjevic T, Hess J, Michiels C, Kietzmann T, and Gorlach A. 2007. Reactive oxygen species activate the HIF-1alpha promoter via a functional NFkappaB site. Arterioscler Thromb Vasc Biol 27: 755–761. [PubMed: 17272744]
5. Kumar S, Marathe S, Dhamija B, Zambare U, Bilala R, Warang S, Nayak C, and Purwar R. 2021. Presence and the roles of IL-9/Th9 axis in vitiligo. Pigment cell & melanoma research 34: 966–972. [PubMed: 33834624]
6. Purwar R, Schlapbach C, Xiao S, Kang HS, Elyaman W, Jiang X, Jetten AM, Khoury SJ, Fuhlbrigge RC, Kuchroo VK, Clark RA, and Kupper TS 2012. Robust tumor immunity to melanoma mediated by interleukin-9-producing T cells. Nature medicine 18: 1248–1253.
7. Nograles KE, Zaba LC, Guttman-Yassky E, Fuentes-Duculan J, Suarez-Farinas M, Cardinale I, Khatcherian A, Gonzalez J, Pierson KC, White TR, Pensabene C, Coats I, Novitskaya I, Lowes MA, and Krueger JG 2008. Th17 cytokines interleukin (IL)-17 and IL-22 modulate distinct inflammatory and keratinocyte-response pathways. The British journal of dermatology 159: 1092–1102. [PubMed: 18684158]
8. Hawkes JE, Yan BY, Chan TC, and Krueger JG 2018. Discovery of the IL-23/IL-17 Signaling Pathway and the Treatment of Psoriasis. Journal of immunology 201: 1605–1613.
9. Fletcher JM, Moran B, Petrasca A, and Smith CM 2020. IL-17 in inflammatory skin diseases psoriasis and hidradenitis suppurativa. Clin Exp Immunol 201: 121–134. [PubMed: 32379344]
10. Liu T, Li S, Ying S, Tang S, Ding Y, Li Y, Qiao J, and Fang H. 2020. The IL-23/IL-17 Pathway in Inflammatory Skin Diseases: From Bench to Bedside. Frontiers in immunology 11: 594735. [PubMed: 33281823]
11. Singh RK, Lee KM, Vujkovic-Cvijin I, Ucmak D, Farahnik B, Abrouk M, Nakamura M, Zhu TH, Bhutani T, Wei M, and Liao W. 2016. The role of IL-17 in vitiligo: A review. Autoimmunity reviews 15: 397–404. [PubMed: 26804758]
12. Monin L, Gudjonsson JE, Childs EE, Amatya N, Xing X, Verma AH, Coleman BM, Garg AV, Killeen M, Mathers A, Ward NL, and Gaffen SL 2017. MCPIP1/Regnase-1 Restricts IL-17A- and IL-17C-Dependent Skin Inflammation. Journal of immunology 198: 767–775.
13. Sugaya M. 2020. The Role of Th17-Related Cytokines in Atopic Dermatitis. International journal of molecular sciences 21:1314. [PubMed: 32075269]
14. Marzano AV, Ortega-Loayza AG, Heath M, Morse D, Genovese G, and Cugno M. 2019. Mechanisms of Inflammation in Neutrophil-Mediated Skin Diseases. Frontiers in immunology 10: 1059. [PubMed: 31139187]

15. Speeckaert R, Lambert J, Grine L, Van Gele M, De Schepper S, and van Geel N. 2016. The many faces of interleukin-17 in inflammatory skin diseases. The British journal of dermatology 175: 892–901. [PubMed: 27117954]

16. Blauvelt A, and Chiricozzi A. 2018. The Immunologic Role of IL-17 in Psoriasis and Psoriatic Arthritis Pathogenesis. Clin Rev Allergy Immunol 55: 379–390. [PubMed: 30109481]

17. Mosca M, Hong J, Hadeler E, Hakimi M, Liao W, and Bhutani T. 2021. The Role of IL-17 Cytokines in Psoriasis. Immunotargets Ther 10: 409–418. [PubMed: 34853779]

18. Revu S, Wu J, Henkel M, Rittenhouse N, Menk A, Delgoffe GM, Poholek AC, and McGeachy MJ 2018. IL-23 and IL-1beta Drive Human Th17 Cell Differentiation and Metabolic Reprogramming in Absence of CD28 Costimulation. Cell reports 22: 2642–2653. [PubMed: 29514093]

19. Ghanemi A, and St-Amand J. 2018. Interleukin-6 as a “metabolic hormone”. Cytokine 112: 132–136. [PubMed: 29983356]

20. Baixauli F, Piletic K, Puleston DJ, Villa M, Field CS, Flachsmann LJ, Quintana A, Rana N, Edwards-Hicks J, Matsushita M, Stanczak MA, Grzes KM, Kabat AM, Fabri M, Caputa G, Kelly B, Corrado M, Musa Y, Duda KJ, Mittler G, O’Sullivan D, Sesaki H, Jenuwein T, Buescher JM, Pearce EJ, Sanin DE, and Pearce EL 2022. An LKB1-mitochondria axis controls T(H)17 effector function. Nature 610: 555–561. [PubMed: 36171294]

21. Belguendouz H, Lahmar-Belguendouz K, Messaoudene D, Djeraba Z, Otmani F, Hakem D, Lahlou-Boukoffa OS, Youinou P, and Touil-Boukoffa C. 2015. Cytokines Modulate the “Immune-Metabolism” Interactions during Behcet Disease: Effect on Arginine Metabolism. Int J Inflam 2015: 241738.

22. Alwarawrah Y, Kiernan K, and MacIver NJ 2018. Changes in Nutritional Status Impact Immune Cell Metabolism and Function. Front Immunol 9: 1055. [PubMed: 29868016]

23. Ganeshan K, and Chawla A. 2014. Metabolic regulation of immune responses. Annu Rev Immunol 32: 609–634. [PubMed: 24655299]

24. Kumar S, Dhamija B, Attrish D, Sawant V, Sengar M, Thorat J, Shet T, Jain H, and Purwar R. 2022. Genetic alterations and oxidative stress in T cell lymphomas. Pharmacology & therapeutics 236: 108109. [PubMed: 35007658]

25. Marathe S, Dhamija B, Kumar S, Jain N, Ghosh S, Dharikar JP, Srinivasan S, Das S, Sawant A, Desai S, Khan F, Syiemlieh A, Munde M, Nayak C, Gandhi M, Kumar A, Srivastava S, Venkatesh KV, Barthel SR, and Purwar R. 2021. Multiomics Analysis and Systems Biology Integration Identifies the Roles of IL-9 in Keratinocyte Metabolic Reprogramming. The Journal of investigative dermatology 141: 1932–1942. [PubMed: 33667432]

26. Wickersham M, Wachtel S, Wong Fok Lung T, Soong G, Jacquet R, Richardson A, Parker D, and Prince A. 2017. Metabolic Stress Drives Keratinocyte Defenses against Staphylococcus aureus Infection. Cell reports 18: 2742–2751. [PubMed: 28297676]

27. Cai Y, Xue F, Qin H, Chen X, Liu N, Fleming C, Hu X, Zhang HG, Chen F, Zheng J, and Yan J. 2019. Differential Roles of the mTOR-STAT3 Signaling in Dermal gammadelta T Cell Effector Function in Skin Inflammation. Cell reports 27: 3034–3048 e3035. [PubMed: 31167146]

28. O’Neill LA, and Pearce EJ 2016. Immunometabolism governs dendritic cell and macrophage function. The Journal of experimental medicine 213: 15–23. [PubMed: 26694970]

29. Roux C, Mucciolo G, Kopecka J, Novelli F, Riganti C, and Cappello P. 2021. IL17A Depletion Affects the Metabolism of Macrophages Treated with Gemcitabine. Antioxidants (Basel) 10.

30. Dragon S, Saffar AS, Shan L, and Gounni AS 2008. IL-17 attenuates the anti-apoptotic effects of GM-CSF in human neutrophils. Mol Immunol 45: 160–168. [PubMed: 17555818]

31. Majumder S, Amatya N, Revu S, Jawale CV, Wu D, Rittenhouse N, Menk A, Kupul S, Du F, Raphael I, Bhattacharjee A, Siebenlist U, Hand TW, Delgoffe GM, Poholek AC, Gaffen SL, Biswas PS, and McGeachy MJ 2019. IL-17 metabolically reprograms activated fibroblastic reticular cells for proliferation and survival. Nature immunology 20: 534–545. [PubMed: 30962593]

32. Zuniga LA, Shen WJ, Joyce-Shaikh B, Pyatnova EA, Richards AG, Thom C, Andrade SM, Cua DJ, Kraemer FB, and Butcher EC 2010. IL-17 regulates adipogenesis, glucose homeostasis, and obesity. Journal of immunology 185: 6947–6959.

33. Bechara R, McGeachy MJ, and Gaffen SL 2021. The metabolism-modulating activity of IL-17 signaling in health and disease. The Journal of experimental medicine 218:e20202191.
34. Lou F, Sun Y, Xu Z, Niu L, Wang Z, Deng S, Liu Z, Zhou H, Bai J, Yin Q, Cai X, Sun L, Wang H, Li Q, Wu Z, Chen X, Gu J, Shi YL, Tao W, Ginhoux F, and Wang H. 2020. Excessive Polyamine Generation in Keratinocytes Promotes Self-RNA Sensing by Dendritic Cells in Psoriasis. Immunity 53: 204–216 e210. [PubMed: 32553276]
35. Bandyopadhyay M, and Larregina AT 2020. Keratinocyte-Polyamines and Dendritic Cells: A Bad Duet for Psoriasis. Immunity 53: 16–18. [PubMed: 32668224]
36. Zhang Z, Zi Z, Lee EE, Zhao J, Contreras DC, South AP, Abel ED, Chong BF, Vandergriff T, Hosler GA, Scherer PE, Mettlen M, Rathmell JC, DeBerardinis RJ, and Wang RC 2018. Differential glucose requirement in skin homeostasis and injury identifies a therapeutic target for psoriasis. Nature medicine 24: 617–627.
37. Elpelt A, Albrecht S, Teutloff C, Huging M, Saeidpour S, Lohan SB, Hedtrich S, and Meinke MC 2019. Insight into the redox status of inflammatory skin equivalents as determined by EPR spectroscopy. Chem Biol Interact 310: 108752. [PubMed: 31330126]
38. Pastore S, and Korkina L. 2010. Redox imbalance in T cell-mediated skin diseases. Mediators Inflamm 2010: 861949. [PubMed: 20847812]
39. Wagener FA, Carels CE, and Lundvig DM 2013. Targeting the redox balance in inflammatory skin conditions. Int J Mol Sci 14: 9126–9167. [PubMed: 23624605]
40. Nakai K, and Tsuruta D. 2021. What Are Reactive Oxygen Species, Free Radicals, and Oxidative Stress in Skin Diseases? Int J Mol Sci 22:10799. [PubMed: 34639139]
41. Plenkowska J, Gabig-Ciminska M, and Mozolewski P. 2020. Oxidative Stress as an Important Contributor to the Pathogenesis of Psoriasis. Int J Mol Sci 21:6206. [PubMed: 32867343]
42. Wronski A, and Wojcik P. 2022. Impact of ROS-Dependent Lipid Metabolism on Psoriasis Pathophysiology. Int J Mol Sci 23:12137. [PubMed: 36292991]
43. Hubackova S, Kucerova A, Michlits G, Kyjacova L, Reinis M, Korolov O, Bartek J, and Hodny Z. 2016. IFNgamma induces oxidative stress, DNA damage and tumor cell senescence via TGFbeta/SMAD signaling-dependent induction of Nox4 and suppression of ANT2. Oncogene 35: 1236–1249. [PubMed: 25982278]
44. Page MJ, Bester J, and Pretorius E. 2018. The inflammatory effects of TNF-alpha and complement component 3 on coagulation. Sci Rep 8: 1812. [PubMed: 29379088]
45. Huang H, Kim HJ, Chang EJ, Lee ZH, Hwang SJ, Kim HM, Lee Y, and Kim HH 2009. IL-17 stimulates the proliferation and differentiation of human mesenchymal stem cells: implications for bone remodeling. Cell Death Differ 16: 1332–1343. [PubMed: 19543237]
46. Nadeem A, Ahmad SF, Attia SM, Bakheet SA, Al-Harbi NO, and Al-Ayadhi LY 2018. Activation of IL-17 receptor leads to increased oxidative inflammation in peripheral monocytes of autistic children. Brain Behav Immun 67: 335–344. [PubMed: 28935156]
47. Xu X, Zhang S, Song X, Hu Q, and Pan W. 2018. IL-17 enhances oxidative stress in hepatocytes through Nrf2/keap1 signal pathway activation. Int J Clin Exp Pathol 11: 3318–3323. [PubMed: 31949707]
48. Muri J, and Kopf M. 2021. Redox regulation of immunometabolism. Nat Rev Immunol 21: 363–381. [PubMed: 33340021]
49. Das S, Srinivasan S, Srivastava A, Kumar S, Das G, Das S, Dwivedi A, Karulkar A, Makkad K, Bilala R, Gupta A, Sawant A, Nayak C, Tayalia P, and Purwar R. 2019. Differential Influence of IL-9 and IL-17 on Actin Cytoskeleton Regulates the Migration Potential of Human Keratinocytes. Journal of immunology 202: 1949–1961.
50. Mogha P, Srivastava A, Kumar S, Das S, Kureel S, Dwivedi A, Karulkar A, Jain N, Sawant A, Nayak C, Majumder A, and Purwar R. 2019. Hydrogel scaffold with substrate elasticity mimicking physiological-niche promotes proliferation of functional keratinocytes. RSC advances 9: 10174–10183. [PubMed: 31304009]
51. Roy T, Banang-Mbeumi S, Boateng ST, Ruiz EM, Chamcheu RN, Kang L, King JA, Walker AL, Nagalo BM, Kousoulas KG, Esnault S, Huang S, and Chamcheu JC 2022. Dual targeting of mTOR/IL-17A and autophagy by fisetin alleviates psoriasis-like skin inflammation. Front Immunol 13: 1075804. [PubMed: 36741386]

52. Shi X, Jin L, Dang E, Chang T, Feng Z, Liu Y, and Wang G. 2011. IL-17A upregulates keratin 17 expression in keratinocytes through STAT1- and STAT3-dependent mechanisms. The Journal of investigative dermatology 131: 2401–2408. [PubMed: 21796151]

53. Tu J, Yin Z, Guo J, He F, Long F, and Yin Z. 2020. Acitretin inhibits IL-17A-induced IL-36 expression in keratinocytes by down-regulating IkappaBzeta. Int Immunopharmacol 79: 106045. [PubMed: 31863918]

54. Xu X, Prens E, Florencia E, Leenen P, Boon L, Asmawidjaja P, Mus AM, and Lubberts E. 2021. Interleukin-17A Drives IL-19 and IL-24 Expression in Skin Stromal Cells Regulating Keratinocyte Proliferation. Front Immunol 12: 719562. [PubMed: 34616394]

55. Alkhilaiwi F, Wang L, Zhou D, Raudsepp T, Ghosh S, Paul S, Palechor-Ceron N, Brandt S, Luff J, Liu X, Schlegel R, and Yuan H. 2018. Long-term expansion of primary equine keratinocytes that maintain the ability to differentiate into stratified epidermis. Stem Cell Res Ther 9: 181. [PubMed: 29973296]

56. Rai V, Muthuraj M, Gandhi MN, Das D, and Srivastava S. 2017. Real-time iTRAQ-based proteome profiling revealed the central metabolism involved in nitrogen starvation induced lipid accumulation in microalgae. Sci Rep 7: 45732. [PubMed: 28378827]

57. Sharma S, Ray S, Moiyadi A, Sridhar E, and Srivastava S. 2014. Quantitative proteomic analysis of meningiomas for the identification of surrogate protein markers. Sci Rep 4: 7140. [PubMed: 25413266]

58. Scopes RK 1974. Measurement of protein by spectrophotometry at 205 nm. Anal Biochem 59: 277–282. [PubMed: 4407487]

59. Smith AC, Eyassu F, Mazat JP, and Robinson AJ 2017. MitoCore: a curated constraint-based model for simulating human central metabolism. BMC Syst Biol 11: 114. [PubMed: 29178872]

60. Orth J, Thiele I. & Palsson B. 2010. What is flux balance analysis? Nature Biotechnology: 245–248.

61. Ebrahim A, Lerman JA, Palsson BO et al. 2013. COBRApy: COnstraints-Based Reconstruction and Analysis for Python. BMC Systems Biology 7: 1–6. [PubMed: 23280066]

62. Holt V, Moren B, Fryklund C, Colbert RA, and Stenkula KG 2023. Acute cytokine treatment stimulates glucose uptake and glycolysis in human keratinocytes. Cytokine 161: 156057. [PubMed: 36208532]

63. Kumar S, Dhamija B, Marathe S, Ghosh S, Dwivedi A, Karulkar A, Sharma N, Sengar M, Sridhar E, Bonda A, Thorat J, Tembhare P, Shet T, Gujral S, Bagal B, Laskar S, Jain H, and Purwar R. 2020. The Th9 Axis Reduces the Oxidative Stress and Promotes the Survival of Malignant T Cells in Cutaneous T-Cell Lymphoma Patients. Molecular cancer research : MCR 18: 657–668. [PubMed: 31996468]

64. Nemecz M, Constantin A, Dumitrescu M, Alexandru N, Filippi A, Tanko G, and Georgescu A. 2018. The Distinct Effects of Palmitic and Oleic Acid on Pancreatic Beta Cell Function: The Elucidation of Associated Mechanisms and Effector Molecules. Frontiers in pharmacology 9: 1554. [PubMed: 30719005]

65. Huang X, Liu Y, Wang Y, Bailey C, Zheng P, and Liu Y. 2021. Dual Targeting Oncoproteins MYC and HIF1alpha Regresses Tumor Growth of Lung Cancer and Lymphoma. Cancers (Basel) 13:694. [PubMed: 33572152]

66. Veras FP, Publio GA, Melo BM, Prado DS, Norbiato T, Cecilio NT, Hiroki C, Damasceno LEA, Jung R, Toller-Kawahisa JE, Martins TV, Assuncao SF, Lima D, Alves MG, Vieira GV, Tavares LA, Alves-Rezende ALR, Karbach SH, Nakaya HI, Cunha TM, Souza CS, Cunha FQ, Sales KU, Waisman A, and Alves-Filho JC 2022. Pyruvate kinase M2 mediates IL-17 signaling in keratinocytes driving psoriatic skin inflammation. Cell reports 41: 111897. [PubMed: 36577385]

67. Ray PD, Huang BW, and Tsuji Y. 2012. Reactive oxygen species (ROS) homeostasis and redox regulation in cellular signaling. Cellular signalling 24: 981–990. [PubMed: 22286106]

68. Li X, Bechara R, Zhao J, McGeachy MJ, and Gaffen SL 2019. IL-17 receptor-based signaling and implications for disease. Nature immunology 20: 1594–1602. [PubMed: 31745337]

69. Krueger JG, Wharton KA Jr., Schlitt T, Suprun M, Torene RI, Jiang X, Wang CQ, Fuentes-Duculan J, Hartmann N, Peters T, Koroleva I, Hillenbrand R, Letzkus M, Yu X, Li Y, Glueck A, Hasselberg A, Flannery B, Suarez-Farinas M, and Hueber W. 2019. IL-17A inhibition by secukinumab

induces early clinical, histopathologic, and molecular resolution of psoriasis. J Allergy Clin Immunol 144: 750–763. [PubMed: 31129129]

70. Yan J. 2017. Identifying biomarkers in human psoriasis: revealed by a systems metabolomics approach. The British journal of dermatology 176: 555–557. [PubMed: 28300304]
71. Kang H, Li X, Zhou Q, Quan C, Xue F, Zheng J, and Yu Y. 2017. Exploration of candidate biomarkers for human psoriasis based on gas chromatography-mass spectrometry serum metabolomics. The British journal of dermatology 176: 713–722. [PubMed: 27564527]
72. Friis NU, Hoffmann N, Gyldenlove M, Skov L, Vilsboll T, Knop FK, and Storgaard H. 2019. Glucose metabolism in patients with psoriasis. The British journal of dermatology 180: 264–271. [PubMed: 30376181]
73. Konieczny P, Xing Y, Sidhu I, Subudhi I, Mansfield KP, Hsieh B, Biancur DE, Larsen SB, Cammer M, Li D, Landen NX, Loomis C, Heguy A, Tikhonova AN, Tsirigos A, and Naik S. 2022. Interleukin-17 governs hypoxic adaptation of injured epithelium. Science 377: eabg9302.
74. Huang X, Chen J, Zeng W, Wu X, Chen M, and Chen X. 2019. Membrane-enriched solute carrier family 2 member 1 (SLC2A1/GLUT1) in psoriatic keratinocytes confers sensitivity to 2-deoxy-D-glucose (2-DG) treatment. Exp Dermatol 28: 198–201. [PubMed: 30480843]
75. Chen C, Yi X, Liu P, Li J, Yan B, Zhang D, Zhu L, Yu P, Li L, Zhang J, Kuang Y, Zhao S, Zhu W, Peng C, and Chen X. 2023. CD147 Facilitates the Pathogenesis of Psoriasis through Glycolysis and H3K9me3 Modification in Keratinocytes. Research (Wash D C) 6: 0167. [PubMed: 37303600]
76. Okubo A, Uchida Y, Higashi Y, Sato T, Ogawa Y, Ryuge A, Kadomatsu K, and Kanekura T. 2021. CD147 Is Essential for the Development of Psoriasis via the Induction of Th17 Cell Differentiation. Int J Mol Sci 23:177. [PubMed: 35008603]
77. Gardner LCS, Grantham HJ, and Reynolds NJ 2019. IL-17 May Be a Key Cytokine Linking Psoriasis and Hyperglycemia. The Journal of investigative dermatology 139: 1214–1216. [PubMed: 31126427]
78. Cruzat V, Macedo Rogero M, Noel Keane K, Curi R, and Newsholme P. 2018. Glutamine: Metabolism and Immune Function, Supplementation and Clinical Translation. Nutrients 10.
79. Cibrian D, de la Fuente H, and Sanchez-Madrid F. 2020. Metabolic Pathways That Control Skin Homeostasis and Inflammation. Trends in molecular medicine 26: 975–986. [PubMed: 32371170]
80. Wang MJ, Huang HJ, Xu YY, Vos H, Gulersonmez C, Stigter E, Gerritsen J, Gallego MP, van Es R, Li L, Deng H, Han L, Huang RY, Lu CJ, and Burgering BM 2023. Metabolic rewiring in keratinocytes by miR-31–5p identifies therapeutic intervention for psoriasis. EMBO Mol Med 15: e15674. [PubMed: 36855912]
81. Labow BI, Souba WW, and Abcouwer SF 1999. Glutamine synthetase expression in muscle is regulated by transcriptional and posttranscriptional mechanisms. The American journal of physiology 276: E1136–1145. [PubMed: 10362628]
82. Swindell WR, Remmer HA, Sarkar MK, Xing X, Barnes DH, Wolterink L, Voorhees JJ, Nair RP, Johnston A, Elder JT, and Gudjonsson JE 2015. Proteogenomic analysis of psoriasis reveals discordant and concordant changes in mRNA and protein abundance. Genome medicine 7: 86. [PubMed: 26251673]
83. Jaishy B, and Abel ED 2016. Lipids, lysosomes, and autophagy. Journal of lipid research 57: 1619–1635. [PubMed: 27330054]
84. Diab J, Hansen T, Goll R, Stenlund H, Ahnlund M, Jensen E, Moritz T, Florholmen J, and Forsdahl G. 2019. Lipidomics in Ulcerative Colitis Reveal Alteration in Mucosal Lipid Composition Associated With the Disease State. Inflammatory bowel diseases 25: 1780–1787. [PubMed: 31077307]
85. Salvatore G, Bernoud-Hubac N, Bissay N, Debard C, Daira P, Meugnier E, Proamer F, Hanau D, Vidal H, Arico M, Delprat C, and Mahtouk K. 2015. Human monocyte-derived dendritic cells turn into foamy dendritic cells with IL-17A. J Lipid Res 56: 1110–1122. [PubMed: 25833686]
86. Shen T, Chen X, Li Y, Tang X, Jiang X, Yu C, Zheng Y, Guo H, and Ling W. 2017. Interleukin-17A exacerbates high-fat diet-induced hepatic steatosis by inhibiting fatty acid beta-oxidation. Biochim Biophys Acta Mol Basis Dis 1863: 1510–1518. [PubMed: 28153707]

87. Zhang X, Li X, Wang Y, Chen Y, Hu Y, Guo C, Yu Z, Xu P, Ding Y, Mi QS, Wu J, Gu J, and Shi Y. 2022. Abnormal lipid metabolism in epidermal Langerhans cells mediates psoriasis-like dermatitis. JCI Insight 7:e150223.

88. Ferretti G, Bacchetti T, Campanati A, Simonetti O, Liberati G, and Offidani A. 2012. Correlation between lipoprotein(a) and lipid peroxidation in psoriasis: role of the enzyme paraoxonase-1. The British journal of dermatology 166: 204–207. [PubMed: 21790517]

89. Shih CM, Chen CC, Chu CK, Wang KH, Huang CY, and Lee AW 2020. The Roles of Lipoprotein in Psoriasis. Int J Mol Sci 21:859. [PubMed: 32013194]

90. Xiao Y, Jing D, Tang Z, Peng C, Yin M, Liu H, Chen X, and Shen M. 2022. Serum Lipids and Risk of Incident Psoriasis: A Prospective Cohort Study from the UK Biobank Study and Mendelian Randomization Analysis. The Journal of investigative dermatology 142: 3192–3199 e3112. [PubMed: 35850211]

91. Zeng C, Wen B, Hou G, Lei L, Mei Z, Jia X, Chen X, Zhu W, Li J, Kuang Y, Zeng W, Su J, Liu S, Peng C, and Chen X. 2017. Lipidomics profiling reveals the role of glycerophospholipid metabolism in psoriasis. Gigascience 6: 1–11.

92. Varshney P, Narasimhan A, Mittal S, Malik G, Sardana K, and Saini N. 2016. Transcriptome profiling unveils the role of cholesterol in IL-17A signaling in psoriasis. Sci Rep 6: 19295. [PubMed: 26781963]

93. Papandreou I, Cairns RA, Fontana L, Lim AL, and Denko NC 2006. HIF-1 mediates adaptation to hypoxia by actively downregulating mitochondrial oxygen consumption. Cell Metab 3: 187–197. [PubMed: 16517406]

94. Hayashi Y, Yokota A, Harada H, and Huang G. 2019. Hypoxia/pseudohypoxia-mediated activation of hypoxia-inducible factor-1alpha in cancer. Cancer Sci 110: 1510–1517. [PubMed: 30844107]

95. Yoon J, Juhn KM, Ko JK, Yoon SH, Ko Y, Lee CY, and Lim JH 2013. Effects of oxygen tension and IGF-I on HIF-1alpha protein expression in mouse blastocysts. Journal of assisted reproduction and genetics 30: 99–105. [PubMed: 23232974]

96. Rezvani HR, Ali N, Nissen LJ, Harfouche G, de Verneuil H, Taieb A, and Mazurier F. 2011. HIF-1alpha in epidermis: oxygen sensing, cutaneous angiogenesis, cancer, and non-cancer disorders. The Journal of investigative dermatology 131: 1793–1805. [PubMed: 21633368]

97. Li Y, Su J, Li F, Chen X, and Zhang G. 2017. MiR-150 regulates human keratinocyte proliferation in hypoxic conditions through targeting HIF-1alpha and VEGFA: Implications for psoriasis treatment. PLoS One 12: e0175459.

98. Vasilopoulos Y, Sourli F, Zafiriou E, Klimi E, Ioannou M, Mamuris Z, Simos G, Koukoulis G, and Roussaki-Schulze A. 2013. High serum levels of HIF-1alpha in psoriatic patients correlate with an over-expression of IL-6. Cytokine 62: 38–39. [PubMed: 23517877]

99. Kim JH, Bae HC, Kim J, Lee H, Ryu WI, Son ED, Lee TR, Jeong SH, and Son SW 2018. HIF-1alpha-mediated BMP6 down-regulation leads to hyperproliferation and abnormal differentiation of keratinocytes in vitro. Exp Dermatol 27: 1287–1293. [PubMed: 30230035]

100. Torales-Cardena A, Martinez-Torres I, Rodriguez-Martinez S, Gomez-Chavez F, Cancino-Diaz JC, Vazquez-Sanchez EA, and Cancino-Diaz ME 2015. Cross Talk between Proliferative, Angiogenic, and Cellular Mechanisms Orchestred by HIF-1alpha in Psoriasis. Mediators Inflamm 2015: 607363. [PubMed: 26136626]

101. Tang W, Long T, Li F, Peng C, Zhao S, Chen X, and Su J. 2021. HIF-1alpha may promote glycolysis in psoriasis vulgaris via upregulation of CD147 and GLUT1. Zhong Nan Da Xue Xue Bao Yi Xue Ban 46: 333–344. [PubMed: 33967078]

102. Movafagh S, Crook S, and Vo K. 2015. Regulation of hypoxia-inducible factor-1a by reactive oxygen species: new developments in an old debate. Journal of cellular biochemistry 116: 696–703. [PubMed: 25546605]

103. Liang S, Dong S, Liu W, Wang M, Tian S, Ai Y, and Wang H. 2021. Accumulated ROS Activates HIF-1alpha-Induced Glycolysis and Exerts a Protective Effect on Sensory Hair Cells Against Noise-Induced Damage. Frontiers in molecular biosciences 8: 806650. [PubMed: 35096971]

104. Prussick R, Prussick L, and Gutman J. 2013. Psoriasis Improvement in Patients Using Glutathione-enhancing, Nondenatured Whey Protein Isolate: A Pilot Study. The Journal of clinical and aesthetic dermatology 6: 23–26.

105. Hu J, Bian Q, Ma X, Xu Y, and Gao J. 2022. A double-edged sword: ROS related therapies in the treatment of psoriasis. Asian J Pharm Sci 17: 798–816. [PubMed: 36600897]

106. Emmert H, Fonfara M, Rodriguez E, and Weidinger S. 2020. NADPH oxidase inhibition rescues keratinocytes from elevated oxidative stress in a 2D atopic dermatitis and psoriasis model. Exp Dermatol 29: 749–758. [PubMed: 32640089]

107. Zhang Y, Li Y, Zhou L, Yuan X, Wang Y, Deng Q, Deng Z, Xu S, Wang Q, Xie H, and Li J. 2022. Nav1.8 in keratinocytes contributes to ROS-mediated inflammation in inflammatory skin diseases. Redox Biol 55: 102427. [PubMed: 35952475]

108. Keum H, Kim TW, Kim Y, Seo C, Son Y, Kim J, Kim D, Jung W, Whang CH, and Jon S. 2020. Bilirubin nanomedicine alleviates psoriatic skin inflammation by reducing oxidative stress and suppressing pathogenic signaling. J Control Release 325: 359–369. [PubMed: 32681946]

KEY POINTS

- IL-17A modulates keratinocyte metabolism and proliferation via a ROS-HIF1α axis.
- Inhibition of the keratinocyte-IL-17A axis suppresses pro-proliferative metabolism.
- IL-17A axis downstream effectors are elevated in inflamed psoriatic vs. normal skin.

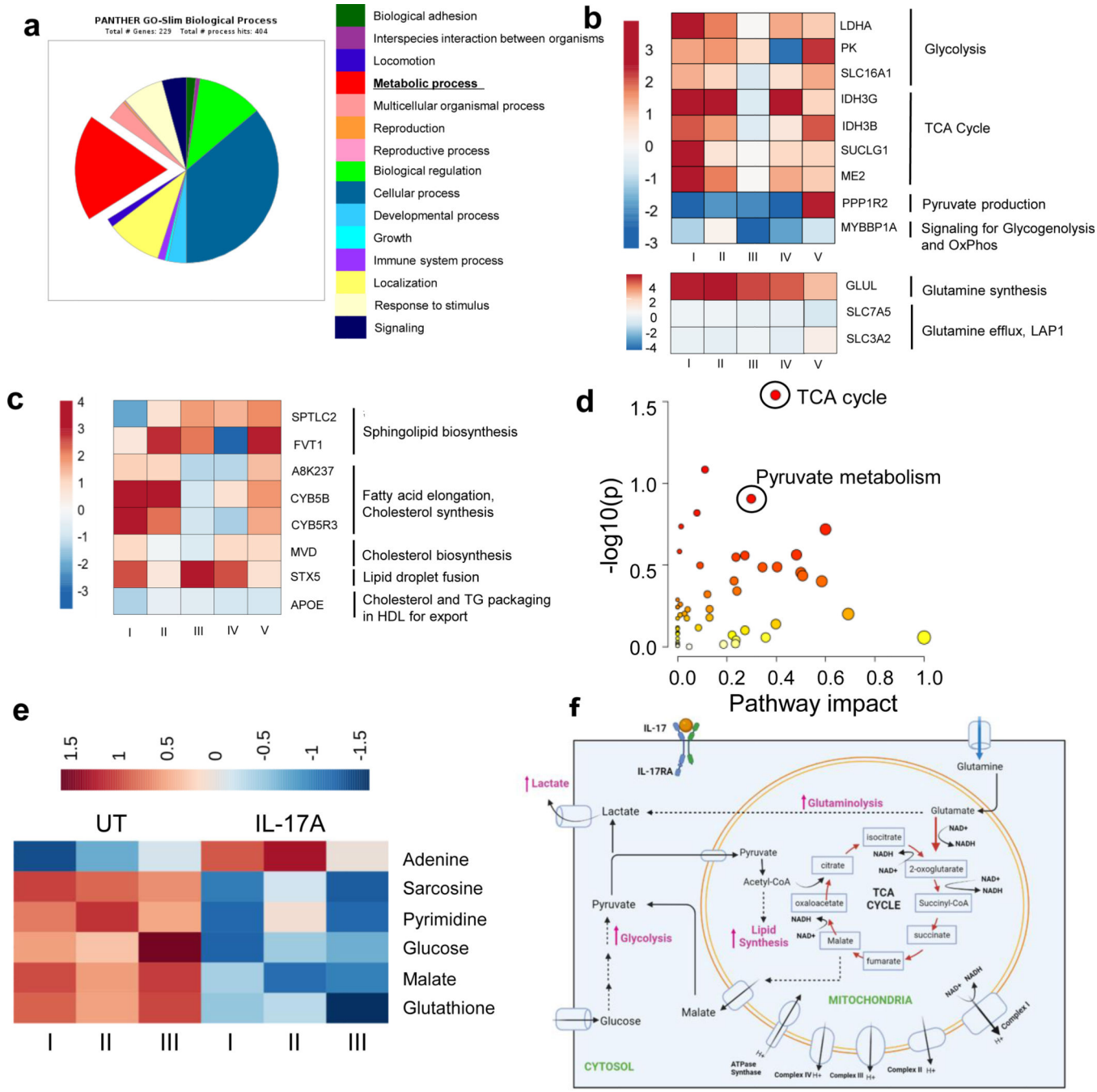

Figure 1. Multiomics and systems biology approaches reveal IL-17A-mediated metabolic reprogramming in human primary keratinocytes.

Human primary keratinocytes (HPKs) obtained from healthy individuals were stimulated with or without IL-17A. **(a)** Pie-chart depicting functional pathways altered in IL-17A-treated versus untreated HPKs ($n = 5$) based on frequencies of differentially expressed ($p < 0.1$) proteins as determined using the PantherDB software. **(b-c)** Heat maps depicting selected dysregulated proteins and their associations with **(b)** carbohydrate and glutamine metabolism and **(c)** lipid metabolism in HPKs. **(d-f)** Cells were lysed and 1H NMR

spectroscopy was performed. Metabolite concentrations were calculated and statistically evaluated using the Metaboanalyst software. Shown are **(d)** major metabolic pathways (color and size increase corresponds to increased effect of the pathway) and **(e)** a heat map of metabolites exhibiting significant changes in response to IL-17A stimulation of HPKs versus unstimulated controls ($n = 3$). **(f)** Schematic representation of dysregulated metabolic pathways and metabolites in HPKs by IL-17A treatment. Solid vertical and dashed arrows represent increased metabolites and pathway flux based on MitoCore modeling.

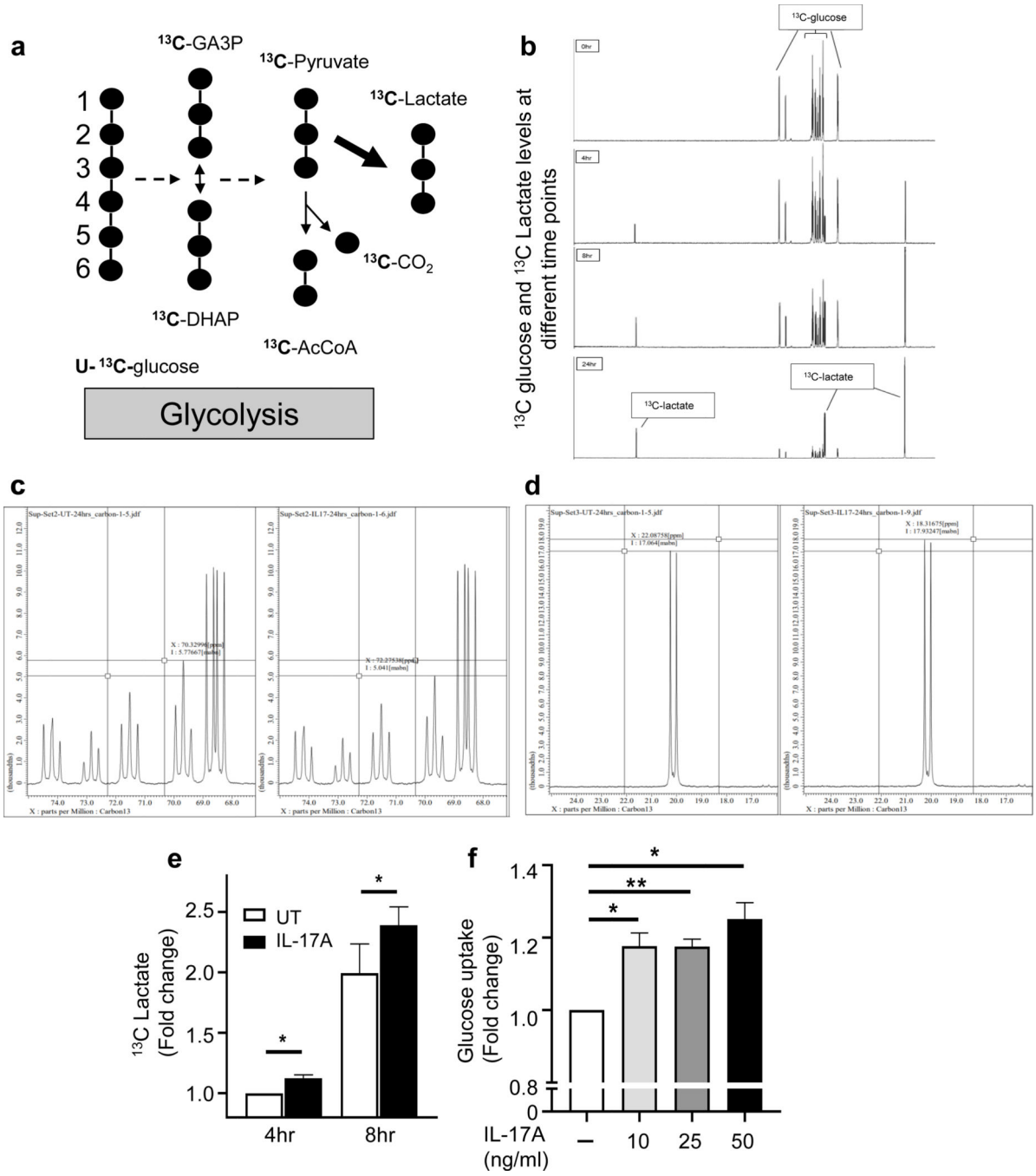

Figure 2. IL-17A regulates glycolytic flux (Warburg-like effect) in human keratinocytes as determined using stable isotope-resolved metabolomics.

Human primary keratinocytes (HPKs) obtained from healthy individuals were stimulated with or without IL-17A. **(a)** Stable isotope-resolved metabolomics was performed using U-^{13}C-labeled glucose as a tracer. **(b)** Spectra of ^{13}C NMR isotope (^{13}C-U-Glc) tracing over different time points in IL-17A-treated HPKs. **(c-d)** ^{13}C NMR spectra depicting **(c)** U-^{13}C-labeled glucose consumption and **(d)** ^{13}C-lactate secretion in HPK supernatants. **(e-f)** 1D ^{1}H and ^{13}C NMR analyses were used to quantify **(e)** ^{13}C lactate production in HPK

supernatants over the indicated time points ($n = 3$). **(f)** Glucose uptake was quantified using a flow cytometer with 2-NBDG at different IL-17A concentrations, viz., 10, 25, and 50 ng/mL ($n = 3$). Results are representative of $n = 3$ independent experiments and values are expressed as mean ± SEM.; ns, not significant, *$p < 0.05$, **$p < 0.01$, ***$p < 0.001$ (Student's paired *t*-test).

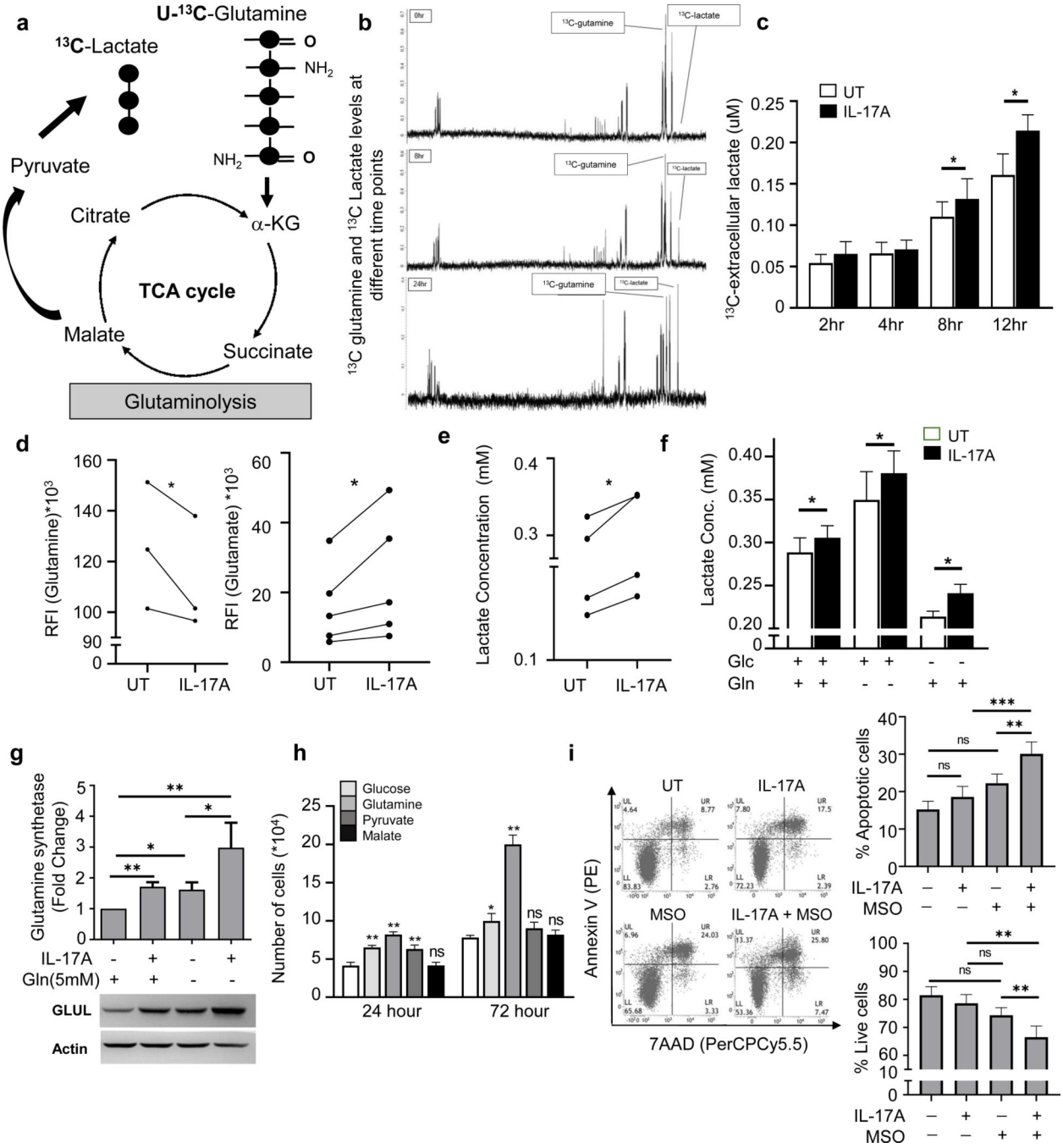

Figure 3. Stable isotope-resolved metabolomics and proteomics unravel IL-17A-dependent regulation of glutamine metabolism in keratinocytes.

Human primary keratinocytes (HPKs) from healthy individuals were stimulated with or without IL-17A. **(a)** Schematic of U-^{13}C-labeled glutamine and ^{13}C-labeled lactate tracers used in stable isotope metabolomics assays for glutaminolysis. **(b)** Spectra of ^{13}C NMR isotope (^{13}C-U-Gln) tracing over different time points in IL-17A-treated HPKs. **(c)** ^{13}C NMR analysis was used to quantify ^{13}C-lactate production in HPK supernatants at different time points (n = 3). **(d)** Luminometric quantification of glutamine and glutamate in

supernatant of IL-17A treated HPKs **(e)** Spectrophotometric quantitation of lactate in HPK supernatants ($n = 4$). **(f)** Contributions of glucose and glutamine toward lactate production in UT versus IL-17A-treated HPKs ($n = 4$) **(g)** Glutamine synthetase expression in absence of glutamine and 5mM of glutamine upon 24hr IL-17A treatment; values are fold changes in mean intensity of bands measured in ImageJ software; hypothesis testing for significance was performed by ratio-paired t-test (n=6). **(h)** Proliferation of IL-17A-treated HPKs in presence of metabolites (glucose: 10mM, glutamine: 4mM, sodium pyruvate: 2mM, Malic acid: 2mM) was analyzed at days 1 and 3 based on trypan blue exclusion of dead cells ($n = 3$). **(i)** Apoptosis of IL-17A-treated HPKs in the presence of myriocin and under glutamine deficient conditions was performed using flow cytometry; percentage of apoptotic cells (Annexin V+ve), percentage of surviving cells (Annexin V-ve, 7AAD-ve). Results are representative of $n = 3–6$ independent experiments and values are expressed as mean ± SEM.; ns, not significant, *$p < 0.05$, **$p < 0.01$, ***$p < 0.001$ (Student's paired *t*-test).

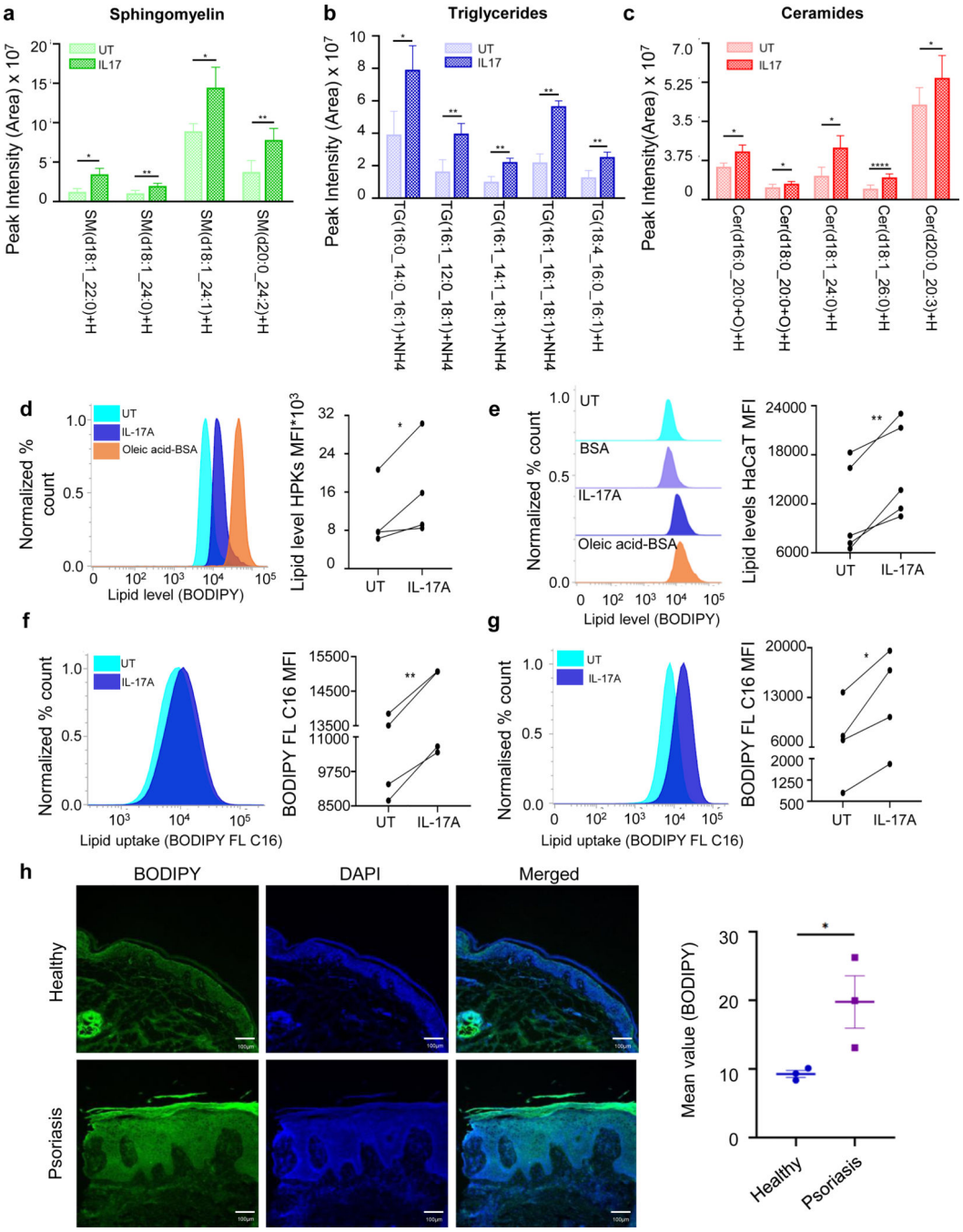

Figure 4. IL-17A stimulates lipid accumulation and fatty acid uptake in human keratinocyte.

Human primary keratinocytes (HPKs) were treated with or without IL-17A (50 ng/mL) for 24 h. **(a-c)** Cells were lysed and metabolites (non-polar) were isolated using methanol/chloroform extraction protocol. Samples were reconstituted in chloroform: methanol (1:1) and lipidomics was performed. Area of different lipid classes were measured and compared. **(d-e)** Intracellular neutral lipid content was measured using flow cytometry with BODIPY (493/503). Shown are representative histogram and cumulative data of BODIPY stained neutral lipid content in **(d)** HPKs and **(e)** HaCaT respectively ($n = 4$). Oleic acid-BSA (200

μM) was used as a positive control. **(f-g)** Lipid uptake in response to IL-17A treatment (24 h) was assessed using flow cytometry with BODIPY FL C16. Shown are representative histogram and cumulative data depicting increased fluorescence in IL-17A-stimulated vs. untreated in **(f)** HPKs and **(g)** HaCaT ($n = 4$) respectively. **(h)** Representative microscopic images and cumulative data of BODIPY (493/503) stained skin biospecimens obtained from healthy and psoriatic individuals (n=3), with nuclei stained by DAPI (magnification 10X). **(**Results are representative of $n = 3–4$ independent experiments and values are expressed as mean ± SEM.; ns, not significant, *$p < 0.05$, **$p < 0.01$, ***$p < 0.001$ (Student's paired *t*-test).

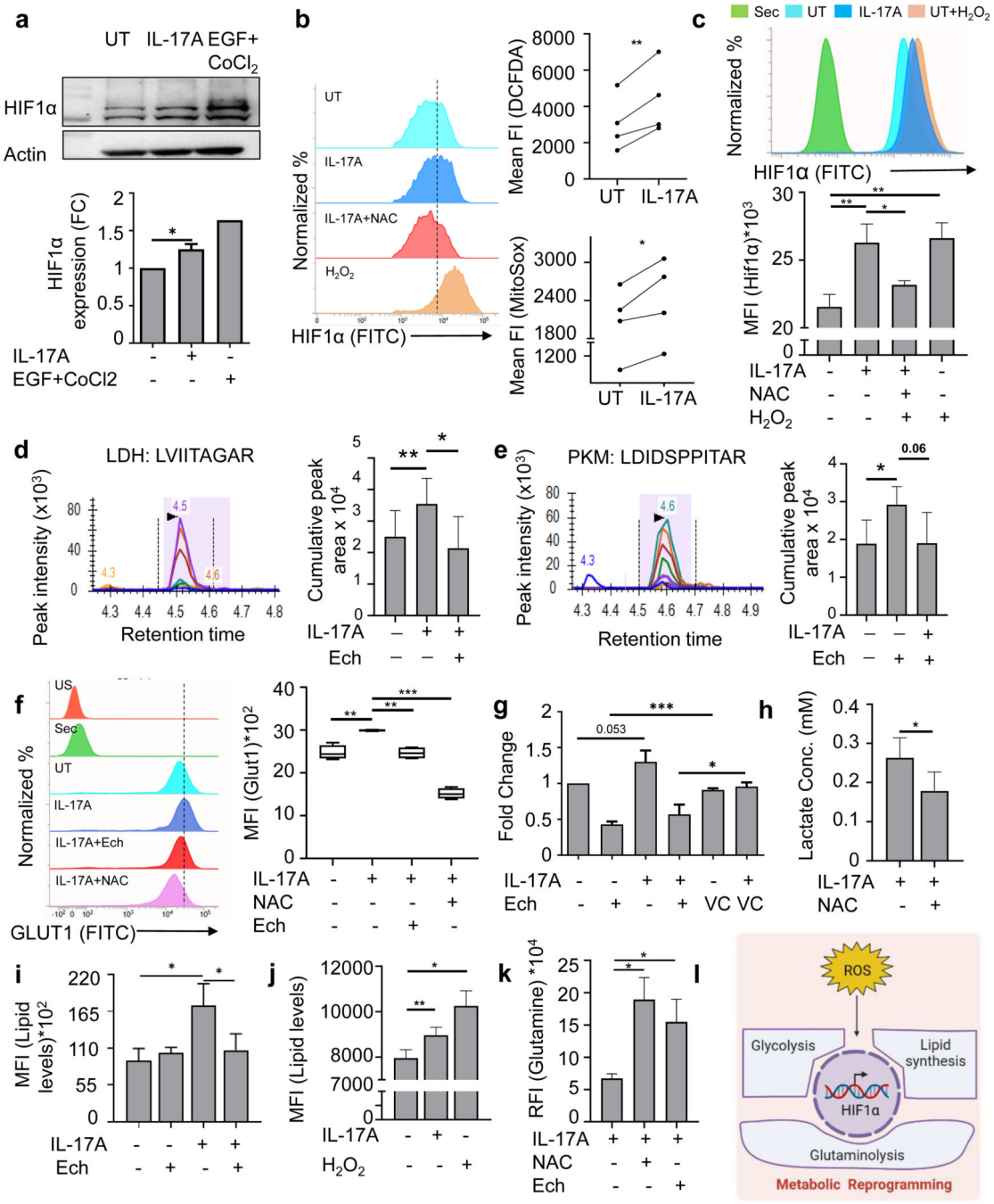

Figure 5. IL-17A modulates redox homeostasis, stimulates ROS-dependent HIF1α expression, and reprograms keratinocyte metabolism

(a) Modulation of HIF1α expression in IL-17A-treated versus Untreated HaCaT cells as measured using western blot analysis ($n = 5$). **(b)** HPKs were stimulated with or without IL-17A, positive control H_2O_2 (50 μmol/L), or negative control N-acetyl cysteine (NAC) for 24 h, and levels of cellular (cROS) and mitochondrial (mROS) were measured using flow cytometry with H2DCFDA **(upper panel)** and MitoSOX **(lower panel)**, respectively. Representative histograms of cROS levels based on H2DCFDA staining (4 h)

and cumulative results from independent experiments ($n = 4$), following 24 h of stimulation. **(c)** Representative flow cytometry histograms and quantitation of ROS-mediated HIF1α expression in HPKs ($n = 6$) **(d-e)** multiple reaction monitoring (MRM) targeted mass spectrometry of **(d)** LDH-A and **(e)** pyruvate kinase in IL-17A and echinomycin treated HPKs. **(f-h)** Effect of IL-17A, echinomycin and NAC-mediated inhibition on **(f)** intracellular GLUT1 expression and **(g-h)** extracellular levels of lactate in HPKs as measured by flow cytometry and spectrophotometrically respectively. **(i-j)** HIF1α and ROS-dependency of intracellular lipid levels in IL-17A stimulated HPKs, evaluated using BODIPY 493/503 ($n = 3$). **(k)** Effect of echinomycin and NAC-mediated inhibition on extracellular glutamine levels in IL-17A treated HPKs (n=3). **(l)** Schematic for ROS-induced HIF1α activation in HPKs leading to metabolic reprogramming of glucose, glutamine and lipid biosynthetic pathways. Results are representative of $n = 3$–6 independent experiments and values are expressed as mean ± SEM.; ns, not significant, $*p < 0.05$, $**p < 0.01$, $***p < 0.001$ (Student's paired *t*-test).

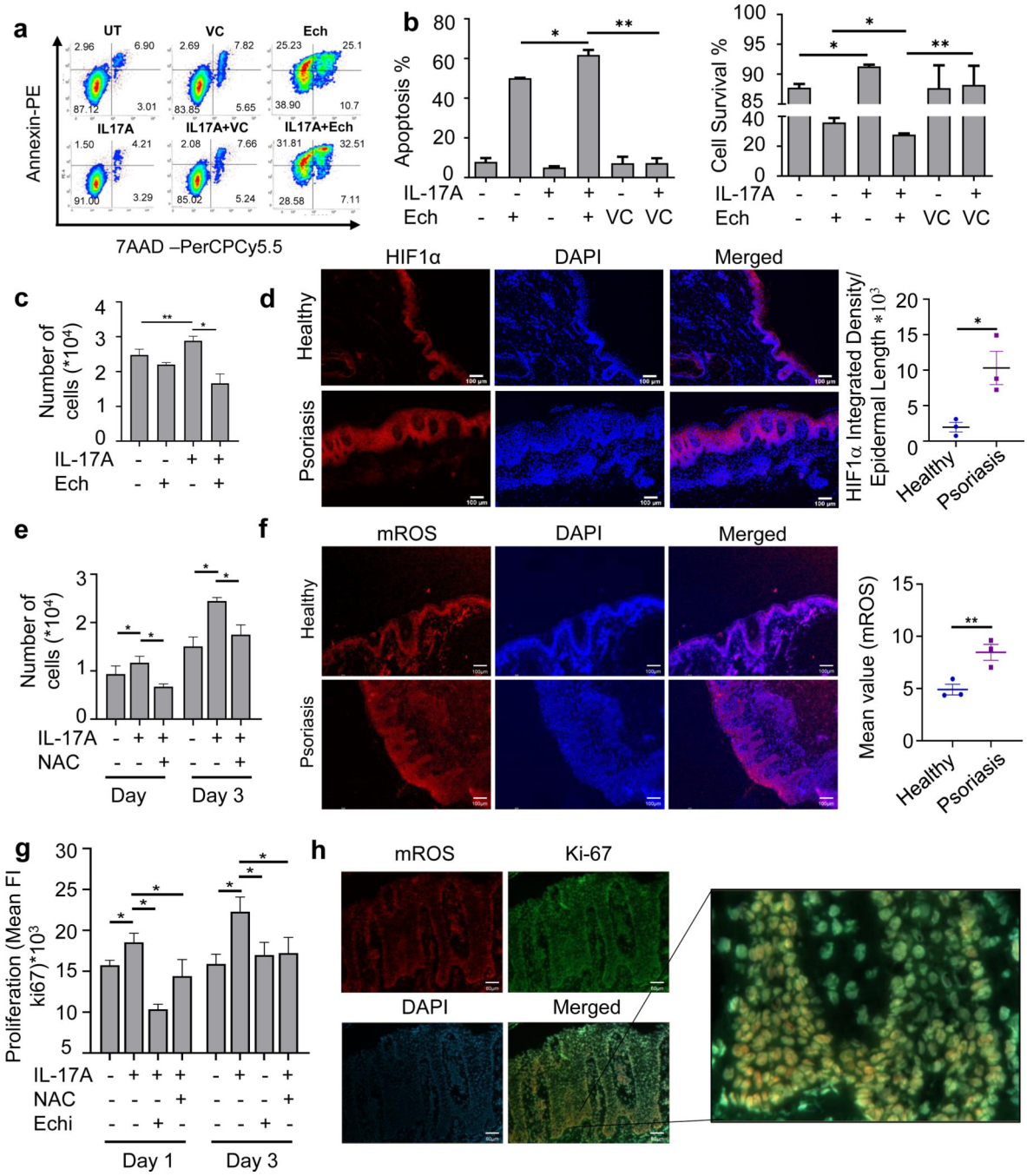

Figure 6. IL-17A triggers ROS-HIF1α-mediated hyperproliferation in psoriasis.

Human primary keratinocytes (HPKs) were treated with or without IL-17A (50 ng/mL). **(a-b)** Frequencies of apoptotic versus live HPKs were assessed by flow cytometry of Annexin V- and 7AAD-stained cells ($n = 5$). Graphs represent percent live (AnnexinV-ve/7AAD-ve) and dead cells (7AAD+ve). **(c)** Effect of IL-17A and echinomycin-mediated HIF1α inhibition on proliferation of HPK cells was analyzed over 24 h and quantified using trypan blue exclusion assay ($n = 3$) **(d)** HIF1α expression in skin biopsies of psoriasis patients ($n = 3$) versus healthy individuals ($n = 3$) was assessed using immunofluorescence. **(e)** ROS-

mediated proliferation of HPKs was analyzed at days 1 and 3 based on trypan blue exclusion of dead cells ($n = 3$). **(f)** Analysis of mROS levels in biopsies obtained from psoriasis patients ($n = 3$) and healthy individuals ($n = 3$). Staining intensity was measured using the ImageJ software and expressed as mean fluorescence intensity/area. **(g)** Effect of IL-17A, echinomycin and NAC on Ki-67 expression in HPKs was measured using flow-cytometry (n-4) **(h)** Immunofluorescence staining of psoriatic skin biopsies showing co-expression of Ki-67 and mROS in basal layer of epidermis at 10X and 40X magnification. All results are representative of $n = 3–4$ independent experiments and values are expressed as mean ± SEM.; ns, not significant, $*p < 0.05$, $**p < 0.01$, $***p < 0.001$ (Student's *t*-test).

Table 1.

Donor information for keratinocyte cell isolates and for healthy and psoriatic patient skin biospecimens.

Sample	Sample ID	Age	Gender	Location
Keratinocytes isolated from healthy skin donors				
a,*b*1	P-105	27	F	Thigh
a,*b*2	P-106	18	M	Thigh
*b*3	P-113	22	F	Neck
4	P-114	29	M	Malar area
5	P-115	48	F	Periumbilical
*a*6	P-116	35	M	Back
7	P-117	28	M	Thigh
8	P-118	20	M	Malar area
9	P-119	37	M	Sebaceous cyst
10	P-120	37	F	Thigh
11	P-121	25	F	Back
12	P-124	37	M	Thigh
*a*13	P-125	47	M	Thigh
*a*14	P-127	35	M	Back
15	P-129	41	F	Thigh
16	P-131	29	M	Malar area
17	P-132	34	M	Thigh
18	P-134	22	M	Back
19	P-135	46	F	Skin
20	P-138	32	F	Scar forehead
21	P-139	36	F	Cyst
22	P-140	60	F	Thigh
23	P-141	48	F	Thigh
24	P-142	41	M	Thigh
25	P-143	36	M	Left eyebrow
26	P-144	40	M	Back
27	P-145	49	M	Back
28	P-146	26	M	Thigh
29	P-147	35	M	Thigh
Skin Biopsies from Healthy Donors				
1	H1	45	M	Left arm
2	H2	22	F	Back
3	H3	35	M	Face
Skin Biopsies from Psoriasis Donors				
1	PSP1	50	M	Scalp

Sample	Sample ID	Age	Gender	Location
2	PSP2	15	F	Right Forearm
3	PSP3	22	M	Back

[a] used in proteomics-based analyses,

[b] used in metabolic-based analyses